scientific reports

Check for updates

OPEN

Utilizing fractional-order operator to Alzheimer's disease dynamics

Kottakkaran Sooppy Nisar[1]✉ & Muhammad Farman[2,3]

Fractional derivative modeling has become an important tool for studying and forecasting disease transmission dynamics. We propose a new mathematical model for Alzheimer's disease, a condition in which dying and malfunctioning neurons impair memory. The model has a five-dimensional set of nonlinear fractional differential equations for microglia, amyloid-beta, tau protein, infected neurons, and functioning neurons. To further understand the dynamics of the proposed model, we demonstrated the solutions' existence, uniqueness, positivity, and feasible domain. We used the next-generation technique to calculate the fundamental reproduction number ($\mathscr{R}_0$), the threshold parameter of Alzheimer's disease transmission. Two model equilibrium points have been found. The reproductive number parameters are subjected to sensitivity analysis in order to show how $\mathscr{R}_0$ responds to parameter changes. The Ulam-Hyers-Rassias stability requirements have been confirmed. The suggested model is solved using the Newton polynomial interpolation method with the discretization of the Caputo fractional-order operator. Lastly, simulations are made to investigate the potential effects of factors that prevent the incidence of Alzheimer's disease. The findings show how the proposed method may be able to provide deeper and possibly accurate predictions for the dynamics of Alzheimer's disease, thus leading to more successful public health campaigns.

Keywords Alzheimer's disease, Fractional-order model, Caputo operator, Sensitivity of parameters, ULAM-Hyers-Rassias stability

Brain research is vital for understanding brain disease pathophysiology, which represents 35% of disorders in Europe. Key challenges include assessing disability-adjusted life years[1]. Brain tumors arise from uncontrolled cell growth, emphasizing the need for early detection and targeted therapies. Mathematical models for evaluating solid tumors, such as those addressing proliferation and cellular motility, enhance our understanding of brain tumors, particularly gliomas due to their invasive characteristics[2,3]. Millions of people worldwide suffer from neurodegenerative diseases, which mostly cause cognitive and behavioral impairments. The creation of successful treatments and a deeper comprehension of their mechanisms are crucial[4]. Variations in mitochondrial viscosity are associated with a number of cellular functions and illnesses. The fluorescent probes used today to detect mitochondrial viscosity are not photostable or permeable. Mito-DDP successfully penetrated cell membranes and dyed the cells, demonstrating its potential practical applications, according to confocal laser scanning microscopy[5]. Alzheimer's disease is a neurodegenerative disorder characterized by memory deterioration due to the dysfunction and death of neurons. It influences neuronal and synaptic function, causing abnormalities such as amyloid-beta buildup and tau tangles, which impair synaptic activity and lead to significant brain atrophy[6]. Often viewed as a consequence of aging, it has become a major public health concern due to its socioeconomic impacts and the rising number of cases. Alois Alzheimer's 1906 description highlights pathological signs and disorientation[7]. The US government invested 226 million in 2015 to address Alzheimer's disease, which is expected to impact 131 million people worldwide by 2050, particularly in middle and low-income nations, with annual health care costs surpassing those of cancer and cardiovascular diseases[8].

A mathematical model in[9] explains Alzheimer's disease pathophysiology using differential rate equations, including microglia, astrocytes, neurons, and amyloid-beta, involving seven species and intercellular signaling influences. A prospective cohort study[10] aimed to develop a multiattribute model of the progression of Alzheimer's disease (AD) from moderate to fatal. Researchers analyzed 91 proteins in cerebral fluid or plasma of Alzheimer's patients and cognitively normal controls to mathematically describe disease-specific molecular characteristics[11]. They found a limited number of signaling proteins that can identify Alzheimer's disease and model pathological markers like tau and amyloid-beta levels. Alzheimer's disease patients have decreased expression of brain-derived neurotrophic factor, an essential neurotrophic factor present throughout the brain[12]. The study[13] highlights the

[1]Department of Mathematics, College of Science and Humanities in Al Kharj, Prince Sattam bin Abdulaziz University, Al Kharj, Saudi Arabia. [2]Department of Mathematics, Mathematics Research Center, Near East University, Nicosia 99138, Cyprus, Turkey. [3]Jadara University Research Center, Jadara University, Irbid 21110, Jordan. ✉email: n.sooppy@psau.edu.sa

use of data-driven computer models in Alzheimer's disease research, which are based on experimental data, providing quick insights and testable predictions. These models are continuously developed and improved to capture a significant portion of existing knowledge. The study[14] proposed a mathematical model concentrating on the function of prions in memory impairment, utilizing differential equations to describe the dynamic production of amyloid plaques. The model works with four distinct species. Researchers used transport and diffusion equations to develop a mathematical model for Alzheimer's disease[15]. Gastrodin has antioxidant qualities, protects neurons, and improves brain function. Its effects and mechanisms on Parkinson's disease in a rat model[16] were examined in a study. Another study[17] looked at the role of ceramide in Alzheimer's disease and neuronal aging as well as icariin's possible mitigating effect. Some other contributions related to the mathematical modeling approach for brain disorders are discussed in[18–20], optimizing the treatments and results of brain disorders derived in[21,22].

Fractional operators are now widely used as a common methodology for investigating the spread of epidemics and as a way to solve real-world problems. Fractional calculus has been the subject of numerous published studies, with new developments improving its theoretical and practical aspects. Fractional calculus is a quickly expanding branch of mathematics and is used to model various biological phenomena for disease models, fractional approaches, and modeling concepts for various diseases discussed in[23–25]. In[26], the authors studied the dynamics of hepatitis B transmission with real data. Because of the order of differential equations, it overcomes the drawbacks of classical models based on derivatives and incorporates intricate real-world dynamics. Researchers are increasingly utilizing fractional calculus to tackle these issues. The fractional order model for Parkinson's disease patients is examined in the paper[27], which also suggests an identification method based on the frequency behavior of wheelchair movements.

The fractional dynamic model of a "disabled man-wheelchair" system is also covered in the essay, along with a control technique that takes into account the wheelchair driver's impairment[31]. offers a mathematical model of Alzheimer's disease that takes gender disparities into consideration. Using variable-order fractional temporal derivatives, the model illustrates how cells and aggregation-prone amyloid fibrils change over time. The model also accounts for neuroprotective memory loss, which is particularly common in postmenopausal women due to the dramatic drop in estrogen levels. The study[32] proposed a simpler and more efficient fractional order-based convolutional neural network model that integrates an improved attention mechanism and a new optimization strategy to accurately and effectively classify Alzheimer's disease. Some of the recent research comes up with the artificial neural network techniques to solve various disease models[28–30].

Our research incorporates the amyloid-beta, tau protein, and microglia compartments that contribute to the transmission of Alzheimer's disease, drawing inspiration from the aforementioned publications. This study introduces a novel model that categorizes neurons into functioning and infected types, incorporating the roles of tau protein, amyloid beta, and microglia in neuronal functionality. Notably, this model has not been previously addressed in existing literature. Introducing fractional calculus into Alzheimer's disease mathematical models addresses research deficiencies by accommodating the disease's memory and hereditary characteristics. Unlike standard integer-order models, fractional models accurately represent the non-local and cumulative impacts of Alzheimer's, offering deeper insights into the complex biological processes involved. This paper's structure is as follows: In Sect. 2, we go over the Caputo fractional derivative and review the essential mathematical principles. We describe the development of the suggested fractional order Alzheimer's disease model in Sect. 3. In order to guarantee biological viability and practicality, Sect. 4 provides a thorough analysis that proves the solutions' existence, uniqueness, boundedness, and positivity. The calculation of the basic reproduction number and equilibrium points is examined in Sect. 5. We do sensitivity analysis of several factors in relation to the model's basic reproduction number in Sect. 6. The model is extended to chaos control in Sect. 7. The numerical method is presented in Sect. 7, while the numerical simulations and comments are presented in Sect. 8. The conclusion is finally given in Sect. 9.

Key definitions

Definition 2.1 [33,34] Consider the function $Q(t)$, which is differentiable to the j^{th} derivative. The definition of the Caputo derivative of $Q(t)$ of order $0 < \sigma \leq 1$ is as follows:

$$ {}_0^c D_t^\sigma Q(t) = \frac{d^\sigma}{dt^\sigma} Q(t) = \begin{cases} \frac{1}{\Gamma(j-\sigma)} \int_0^t \frac{Q^j(\varsigma)}{(t-\varsigma)^{\sigma-j+1}} d\varsigma, & \sigma \in (j-1, j), \quad t > 0, \ j \in \mathbb{N}, \\ Q^j(t), & \sigma = j. \end{cases} \tag{1} $$

The Caputo fractional derivative of a constant k is zero, specifically $\frac{d^\sigma}{dt^\sigma} k = 0$ and ensures:

$$ \frac{d^\sigma}{dt^\sigma} t^j \begin{cases} 0, & j \leq \sigma - 1, \\ \frac{\Gamma(j+1) t^{j-\sigma}}{\Gamma(j-\sigma+1)}, & j > \sigma - 1. \end{cases} \tag{2} $$

At $j = 1$, the Eq. (1) is reduced to

$$ {}_0^c D_t^\sigma Q(t) = \frac{1}{\Gamma(1-\sigma)} \frac{d}{dt} \int_0^t (t-\varsigma)^{-\sigma} Q(\varsigma) d\varsigma. \tag{3} $$

Remark 2.1 The Caputo fractional derivative is an ordinary derivative if $\sigma = 1$. Consequently, the ordinary derivative is generalized by the Caputo fractional derivative.

Definition 2.2 The corresponding fractional integral operator is given by[35]

$$ {}^{c}I_t^{\sigma} Q(t) = \frac{1}{\Gamma(\sigma)} \int_0^t (t-\varsigma)^{(\sigma-1)} Q(\varsigma) d\varsigma. \tag{4} $$

Lemma 2.1 [36] The solution to the cauchy problem:

$$ \begin{cases} {}_0^c D_t^{\sigma} Q(t) = \psi(t, Q(t)), & 0 < \sigma \leq 1, \quad t > 0, \\ Q(0) = Q_0, \end{cases} \tag{5} $$

is given by

$$ Q(t) = Q_0 + \frac{1}{\Gamma(\sigma)} \int_0^t (t-\varsigma)^{(\varsigma-1)} \psi(\varsigma, Q(\varsigma)) d\varsigma. \tag{6} $$

Alzheimer's disease model formulation

There are two primary proteins believed to disrupt communication between brain cells: tau and amyloid. This disruption instigates a positive feedback loop that results in increased production of amyloid-beta and abnormal tau[37]. Both amyloid-beta plaques and tau tangles contribute to neuro-inflammation, which can also be triggered by various microbes, including bacteria and viruses[38]. Microglia, the resident innate immune cells of the central nervous system, play a role in disease progression by modifying their physiological functions and activating inflammatory pathways. The presence of toxic amyloid-beta and tau proteins is believed to activate microglia[39]. Microglia tries to clear the toxic proteins as well as widespread debris from dead and dying cells. Chronic inflammation may set in when microglia cannot keep up with all that needs to be cleared, resulting in neuronal dysfunction, injury, and loss.

Based on previous studies, we develop a new mathematical model of Alzheimer's disease including:

- $\mathrm{F}_N(t)$: Functioning neurons;
- $\mathrm{I}_N(t)$: Infected neurons;
- $\mathrm{A}_\beta(t)$: Amyloid-beta;
- $\mathrm{T}_\mu(t)$: Tau protein; and
- $\mathrm{M}_\delta(t)$: Microglia.

We assume that the density of functioning neurons rises with the brain's neuron production rate of Π_N and falls with the proliferation of neurons in the amyloid-beta cascade at a rate of α and due to the natural death of neurons at a rate of ϕ_1. In Alzheimer's disease, the amyloid-beta peptide forms aggregates that deposit as plaques around neuronal cells and brain vasculature. This deposition is associated with the degradation of neuronal function, leading to impaired memory and cognition, such as compromised thinking, speaking, writing, and other day-to-day activities[40]. Beyond innate immunity, microglia, the central nervous system's macrophages, play critical roles in brain growth, preservation, homeostasis, and restoration. Through a variety of interactions, they not only serve as phagocytes but also influence how neurons and glial cells operate. Understanding the mechanisms underlying the early pathophysiology of neurodevelopmental diseases requires an understanding of the factors influencing microglial homeostasis and diversity throughout normal brain development[41]. To illustrate the possible impact of microglia on the development of functional neurons, we introduced a parameter υ. Consequently, the dynamic of active neurons at time t is given by

$$ \mathrm{F}_N(t) = \Pi_N + \rho \mathrm{T}_\mu - \alpha \mathrm{F}_N \mathrm{A}_\beta - \phi_1 \mathrm{F}_N. \tag{7} $$

Amyloid-beta plaques around brain vasculature and neuronal cells are linked to the deterioration of neuronal function. Beta-amyloids are released into plasma and cerebrospinal fluid when secretases cleave the Amyloid-beta protein, which is found on different cell membranes. These beta-amyloids are ingested and misfolded into beta-folded designs, which eventually develop into fibrils and aggregates known as plaques after adhering to neuronal and glial cell receptors at nanomolar concentrations. Beta-amyloids affect brain signaling and memory function as monomers, dimers, or multimers on cell membranes prior to plaque accumulation[42]. Microglia kill the infected neurons at the rate of β_1. Amyloid-beta clears a percentage of infected neurons at a γ rate. Additionally, the normal death rate of ϕ_2 reduces the number of infected neurons. Therefore, we have

$$ \mathrm{I}_N(t) = \alpha \mathrm{F}_N \mathrm{A}_\beta - \beta_1 \mathrm{I}_N \mathrm{M}_\delta - (\gamma + \phi_2) \mathrm{I}_N. \tag{8} $$

By eliminating amyloid-beta, microglia act as the brain's main immune cells, avoiding the plaque development that can damage neurons. We assume that microglia clean amyloid-beta at a rate of β_2. A wide range of peptidases and proteinases, collectively referred to as amyloid-beta-degrading proteases (AβDPs), are capable of proteolytically breaking down the amyloid-beta protein. These proteases are crucial in controlling the levels of endogenous cerebral amyloid-beta under various physiological and pathological circumstances[43]. Amyloid-beta clusters appear first and are followed by a surge in abnormal tau once amyloid-beta has accumulated to a certain level. We suppose that the proteolytic degradation rate of d_β and the tau protein initialization rate of κ by amyloid-beta also reduce the density of amyloid-beta. Consequently, the amyloid-beta density at time t is given by

$$ \mathrm{A}_\beta(t) = \gamma \mathrm{I}_N - \beta_2 \mathrm{A}_\beta \mathrm{M}_\delta - (d_\beta + \kappa) \mathrm{A}_\beta. \tag{9} $$

Tau protein is triggered by amyloid-beta at a κ rate. By internalizing and breaking down tau seeds, microglia perform protective roles that slow the proliferation of tau. We assume that microglia reduce the density of tau protein at a rate of β_3. Cellular mechanisms, such as the ubiquitin-proteasome system, which mostly breaks down soluble tau, control the degradation of tau proteins. Because tau aggregates into toxic structures like tangles and oligomers, which are detrimental to neurons, neurodegeneration results in decreased functional tau concentrations. Therefore, we suppose that the natural rate of tau protein degradation (d_μ) and neurodegeneration also cause a decrease in tau protein concentration. Consequently, tau protein density is expressed as

$$\mathrm{T}_\mu(t) = \kappa \mathrm{A}_\beta - \beta_3 \mathrm{T}_\mu \mathrm{M}_\delta - (d_\mu + \rho)\mathrm{T}_\mu. \tag{10}$$

Microglia are triggered by tau protein, amyloid beta, and infected neurons. By removing protein clumps and pruning malfunctioning synapses, microglia first defend the nervous system. Chronic activation, on the other hand, turns them into a pro-inflammatory state that leads to increased toxic factors, synapse loss, and neuronal death. Apoptosis and necroptosis are two natural cell death processes that microglia experience, which contribute to a constant turnover necessary for preserving brain health. Despite the extended lifespans of microglia, illness can speed up this sluggish pace of cell renewal. We suppose that, at a rate of ϕ_3, natural death lowers the density of microglia. Consequently, the following represents the microglia concentration at time *t*:

$$\mathrm{M}_\delta(t) = (\beta_1 \mathrm{I}_N + \beta_2 \mathrm{A}_\beta + \beta_3 \mathrm{T}_\mu)\mathrm{M}_\delta - \phi_3 \mathrm{M}_\delta. \tag{11}$$

Figure 1 describes the dynamics of Alzheimer's disease based on the stated assumptions.

Memory effects in physical system models are crucial for assessing non-local effects, with integer order differential equations being limited in this regard. Fractional order derivatives, featuring power-law memory kernels, provide a better representation as they account for a state variable's rate of change based on its entire past behavior. The key difference lies in accuracy, where lower fractional order values signify more pronounced memory effects. The Caputo derivative offers a key advantage over the Riemann-Liouville derivative due to its compatibility with standard initial conditions, while the latter requires initial conditions to be expressed in fractional integral form, which is often impractical for various physical systems. Additionally, the Atangana-Baleanu derivative utilizes a non-singular kernel, specifically the Mittag-Leffler function, effectively addressing the singularity issues that arise with the kernels of the Caputo and Riemann-Liouville derivatives. The Caputo fractional derivative is suited for systems with well-defined initial conditions, as it incorporates past states and non-local interactions, thereby integrating memory effects. Its power-law memory kernels improve system stability and numerical simulations. Additionally, it introduces a new parameter allowing for real number orders of derivatives in fractional order systems. Therefore, we examine the Caputo operator model in order to take these dynamical aspects into account. Using first-order Caputo derivatives of order $\sigma, 0 < \sigma \leq 1$, the fractional-order model is introduced as a nonlinear system.

$$\begin{aligned}
{}_0^c D_t^\sigma \mathrm{F}_N(t) &= \Pi_N + \upsilon \mathrm{M}_\delta - \alpha \mathrm{F}_N \mathrm{A}_\beta - \phi_1 \mathrm{F}_N, \\
{}_0^c D_t^\sigma \mathrm{I}_N(t) &= \alpha \mathrm{F}_N \mathrm{A}_\beta - \beta_1 \mathrm{I}_N \mathrm{M}_\delta - (\gamma + \phi_2)\mathrm{I}_N, \\
{}_0^c D_t^\sigma \mathrm{A}_\beta(t) &= \gamma \mathrm{I}_N - \beta_2 \mathrm{A}_\beta \mathrm{M}_\delta - (d_\beta + \kappa)\mathrm{A}_\beta, \\
{}_0^c D_t^\sigma \mathrm{T}_\mu(t) &= \kappa \mathrm{A}_\beta - \beta_3 \mathrm{T}_\mu \mathrm{M}_\delta - (d_\mu + \rho)\mathrm{T}_\mu, \\
{}_0^c D_t^\sigma \mathrm{M}_\delta(t) &= (\beta_1 \mathrm{I}_N + \beta_2 \mathrm{A}_\beta + \beta_3 \mathrm{T}_\mu)\mathrm{M}_\delta - \phi_3 \mathrm{M}_\delta,
\end{aligned} \tag{12}$$

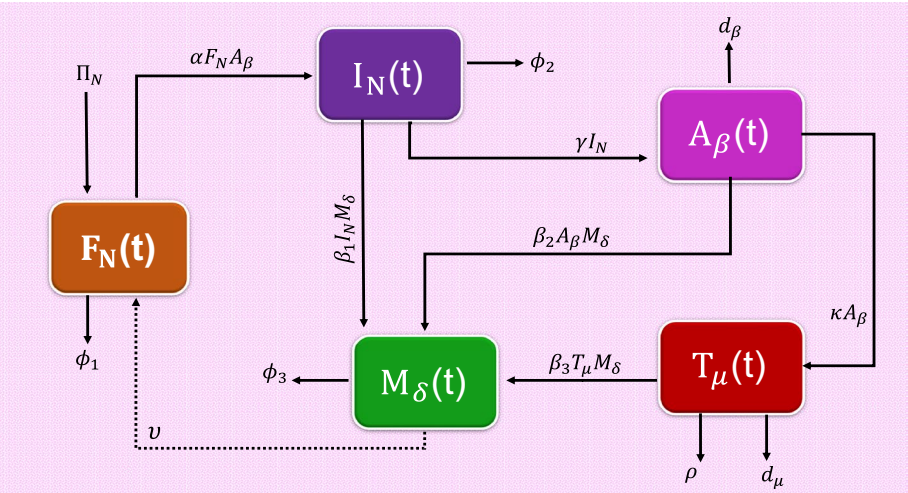

Fig. 1. Flowchart of dynamical system.

where $\sigma \in (0, 1]$ is the derivative order and ${}^{c}D$ is the Caputo fractional derivative.

The initial condition: $\Delta = \{\Lambda_1, \Lambda_2, \Lambda_3, \Lambda_4, \Lambda_5\}$ is stated in the space:

$$\mathbb{C}_+ = \left\{\Delta \in \mathbb{C}([0, \mathrm{T}], \mathbb{R}^5_+) \mid \Lambda_1 = \mathrm{F}_N(\tau),\ \Lambda_1 = \mathrm{I}_N(\tau),\ \Lambda_3 = \mathrm{A}_\beta(\tau),\ \Lambda_4 = \mathrm{T}_\mu(\tau),\ \Lambda_5 = \mathrm{M}_\delta(\tau)\right\}, \quad (13)$$

where $\mathrm{F}_N(0) > 0,\ \mathrm{I}_N(0) > 0,\ \mathrm{A}_\beta(0) > 0,\ \mathrm{T}_\mu(0) > 0,\ \mathrm{M}_\delta(0) > 0$. Also, $\tau \in \mathbb{C}[0, \mathrm{T}]$ and

$$\Lambda_1(\tau) \geq 0, \quad \Lambda_2(\tau) \geq 0, \quad \Lambda_3(\tau) \geq 0, \quad \Lambda_4(\tau) \geq 0, \quad \Lambda_5(\tau) \geq 0. \quad (14)$$

$\mathbb{C}_+$ denotes the Banach space of continuous functions in the domain $[0, \mathrm{T}] \to \mathbb{R}^5_+$, with an appropriate sub-norm and

$$\mathbb{R}^5_+ = \{\mathrm{F}_N, \mathrm{I}_N, \mathrm{A}_\beta, \mathrm{T}_\mu, \mathrm{M}_\delta\}, \qquad \mathrm{F}_N, \mathrm{I}_N, \mathrm{A}_\beta, \mathrm{T}_\mu, \mathrm{M}_\delta \geq 0. \quad (15)$$

Parameters values are given in the Table 1.

Key features analysis

The existence, uniqueness, non-negativity, and boundedness of the suggested model are all investigated in this section.

Existence and uniqueness

Theorem 4.1 [46] There exists a unique solution for every non-negative initial condition in the suggested model (12).

Proof We are evaluating the given model (12)'s solutions for their existence and uniqueness in the region $\Omega \times [0, \mathrm{T}]$, where

$$\Omega = (\mathrm{F}_N, \mathrm{I}_N, \mathrm{A}_\beta, \mathrm{T}_\mu, \mathrm{M}_\delta) \in \mathbb{R}^5 \ : \ \max\left(\|\mathrm{F}_N\|, \|\mathrm{I}_N\|, \|\mathrm{A}_\beta\|, \|\mathrm{T}_\mu\|, \|\mathrm{M}_\delta\|\right). \quad (16)$$

We define the mapping:

$$\mathrm{X}(H) = (\mathrm{X}_1(H), \mathrm{X}_2(H), \mathrm{X}_3(H), \mathrm{X}_4(H), \mathrm{X}_5(H)), \quad (17)$$

where $H = (\mathrm{F}_N, \mathrm{I}_N, \mathrm{A}_\beta, \mathrm{T}_\mu, \mathrm{M}_\delta)$ and

Parameter	Description	Value	Unit	Source
F_N	Functioning brain neurons	0.14	g/ml	[44]
I_N	Infected brain neurons	0	g/ml	[44]
A_β	Amyloid-beta concentration in brain	0.000001	g/ml	[44]
T_μ	Tau protein concentration in brain	0.000001	g/ml	Assumed
M_δ	Microglia concentration in brain	0.02	g/ml	[44]
Π_N	Rate of neuron production in brain	1	Per day	Assumed
υ	Input of microglia on neurons development	0.025	g/ml	Assumed
α	Rate of Amyloid-beta cascade growth in neurons	0.08	Per day	[45]
ϕ_1	Natural death rate of neurons in brain	0.08	Per day	Assumed
β_1	Killing rate of infected neurons by Microglia	0.06	Per day	[44]
γ	Clearance of neurons by Amyloid-beta	0.00017	Per day	[44]
ϕ_2	Death rate of infected neurons	0.00019	Per day	[44]
β_2	Clearance rate of Amyloid-beta by Microglia	0.002	Per day	[44]
d_β	Proteolytic degradation rate of Amyloid-beta	9.51	Per day	[44]
κ	Initiating rate of Tau protein by Amyloid-beta	0.025	Per day	[45]
β_3	Clearance rate of Tau protein by Microglia	0.001	Per day	Assumed
ρ	Rate of Neuro-degeneration from Tau protein	0.025	Per day	[45]
d_μ	Natural degradation rate of tau protein	0.277	Per day	[44]
ϕ_3	Death rate of Microglia	0.015	Per day	[44]

Table 1. Initial variables' states and parameters values.

$$\begin{aligned}
\mathrm{X}_1(H) &= \Pi_N + \upsilon \mathrm{M}_\delta - \alpha \mathrm{F}_N \mathrm{A}_\beta - \phi_1 \mathrm{F}_N, \\
\mathrm{X}_2(H) &= \alpha \mathrm{F}_N \mathrm{A}_\beta - \beta_1 \mathrm{I}_N \mathrm{M}_\delta - (\gamma + \phi_2)\mathrm{I}_N, \\
\mathrm{X}_3(H) &= \gamma \mathrm{I}_N - \beta_2 \mathrm{A}_\beta \mathrm{M}_\delta - (d_\beta + \kappa)\mathrm{A}_\beta, \\
\mathrm{X}_4(H) &= \kappa \mathrm{A}_\beta - \beta_3 \mathrm{T}_\mu \mathrm{M}_\delta - (d_\mu + \rho)\mathrm{T}_\mu, \\
\mathrm{X}_5(H) &= (\beta_1 \mathrm{I}_N + \beta_2 \mathrm{A}_\beta + \beta_3 \mathrm{T}_\mu)\mathrm{M}_\delta - \phi_3 \mathrm{M}_\delta.
\end{aligned} \tag{18}$$

Let $\bar{H} = \left(\bar{\mathrm{F}_N}, \bar{\mathrm{I}_N}, \bar{\mathrm{A}_\beta}, \bar{\mathrm{T}_\mu}, \bar{\mathrm{M}_\delta}\right)$, then

$$\begin{aligned}
\|\mathrm{X}(H) - \mathrm{X}(\bar{H})\| &= |\mathrm{X}_1(H) - \mathrm{X}_1(\bar{H})| + |\mathrm{X}_2(H) - \mathrm{X}_2(\bar{H})| + |\mathrm{X}_3(H) - \mathrm{X}_3(\bar{H})| + |\mathrm{X}_4(H) - \mathrm{X}_4(\bar{H})| \\
&\quad + |\mathrm{X}_5(H) - \mathrm{X}_5(\bar{H})| \\
&\leq -(\alpha \mathrm{A}_\beta + \phi_1)|\mathrm{F}_N - \bar{\mathrm{F}_N}| - (\gamma + \phi_2)|\mathrm{I}_N - \mathrm{I}_N| - (\alpha \mathrm{F}_N + d_\beta + \kappa)|\mathrm{A}_\beta - \bar{\mathrm{A}_\beta}| \\
&\quad - (d_\mu + \rho)|\mathrm{T}_\mu - \bar{\mathrm{T}_\mu}| - \phi_3|\mathrm{M}_\delta - \bar{\mathrm{M}_\delta}| \\
&\leq \mathrm{X}_1|H - \bar{H}| + \mathrm{X}_2|H - \bar{H}| + \mathrm{X}_3|H - \bar{H}| + \mathrm{X}_4|H - \bar{H}| + \mathrm{X}_5|H - \bar{H}| \\
&\leq \mathrm{X}\|H - \bar{H}\|,
\end{aligned} \tag{19}$$

where $\mathrm{X} = \max\{\mathrm{X}_1, \mathrm{X}_2, \mathrm{X}_3, \mathrm{X}_4, \mathrm{X}_5\}$ and

$$\begin{cases}
\mathrm{X}_1 = -\alpha \mathrm{A}_\beta - \phi_1, \\
\mathrm{X}_2 = -\gamma - \phi_2, \\
\mathrm{X}_3 = -\alpha \mathrm{F}_N - d_\beta - \kappa, \\
\mathrm{X}_4 = -d_\mu - \rho, \\
\mathrm{X}_5 = -\phi_3.
\end{cases} \tag{20}$$

The existence and uniqueness of the proposed fractional-order system (12) are thus guaranteed since $\mathrm{X}(H)$ meets the Lipschitz condition. □

Biological feasibility

Examine the closed set Ω for the system (12), which is defined by

$$\Omega = \left\{(\mathrm{X}_1, \mathrm{X}_2, \mathrm{X}_3, \mathrm{X}_4, \mathrm{X}_5) \in \mathbb{R}^+ \ : \ \mathrm{X}_1(t), \mathrm{X}_2(t), \mathrm{X}_3(t), \mathrm{X}_4(t), \mathrm{X}_5(t) \geq 0\right\}, \tag{21}$$

is biological feasible.

Lemma 4.2 [47] Let $q(t) \in \mathbb{C}[0, \mathrm{T}]$ and ${}_0^c D_t^\sigma q(t) \in \mathbb{C}[0, \mathrm{T}]$ for $\sigma \in (0, 1]$. Then, we have

$$q(t) = q(0) + \frac{1}{\Gamma(\sigma)} {}_0^c D_t^\sigma q(t)(t - \varsigma)^\sigma, \tag{22}$$

where $\varsigma \in [0, t]$ for all $t \leq \mathrm{T}$.

Remark 4.1 Let $q(t) \in \mathbb{C}[0, \mathrm{T}]$. and ${}_0^c D_t^\sigma q(t) \geq 0$ for all $t \in (0, \mathrm{T}]$ and $\sigma \in (0, 1]$, it results from Lemma 4.2 that $q(t)$ is non-decreasing for all $t \in [0, \mathrm{T}]$.

Theorem 4.3 [47] $\forall t \geq 0$, the solution of the system (12), starting in $\mathbb{R}_+^5$ and with initial conditions, is constrained and positive invariant.

Proof First, we show the positive invariance of the set Ω. For this reason, it is developed from system (12) that

$$\begin{aligned}
{}_0^c D_t^\sigma \mathrm{F}_N(t)\Big|_{\mathrm{F}_N = 0,\ \mathrm{T}_\mu \geq 0} &= \Pi_N + \upsilon \mathrm{M}_\delta \geq 0, \\
{}_0^c D_t^\sigma \mathrm{I}_N(t)\Big|_{\mathrm{I}_N = 0,\ \mathrm{F}_N \geq 0,\ \mathrm{A}_\beta \geq 0} &= \alpha \mathrm{F}_N \mathrm{A}_\beta \geq 0, \\
{}_0^c D_t^\sigma \mathrm{A}_\beta(t)\Big|_{\mathrm{A}_\beta = 0,\ \mathrm{I}_N \geq 0} &= \gamma \mathrm{I}_N \geq 0, \\
{}_0^c D_t^\sigma \mathrm{T}_\mu(t)\Big|_{\mathrm{T}_\mu = 0,\ \mathrm{A}_\beta \geq 0} &= \kappa \mathrm{A}_\beta \geq 0, \\
{}_0^c D_t^\sigma \mathrm{M}_\delta(t)\Big|_{\mathrm{M}_\delta = 0} &= 0.
\end{aligned} \tag{23}$$

Our conclusion is that the set Ω is positive invariant with respect to model (12) since Lemma 4.2 and system (23) hold for all points of Ω. Next, we establish the boundedness of the set Ω. Adding all of the model's Eq. (12) yields the fractional derivative of the entire population $\mathrm{N}(t)$, namely

$${}_0^c D_t^\sigma \mathrm{N}(t) = \Pi_N - \phi_1 \mathrm{F}_N - \phi_2 \mathrm{I}_N - d_\beta \mathrm{A}_\beta - d_\mu \mathrm{T}_\mu - \phi_3 \mathrm{M}_\delta. \tag{24}$$

Let

$$ {}_0^c D_t^\sigma \mathrm{N}(t) = \Pi_N - \phi_* \mathrm{N}, \tag{25} $$

The problem is reformulated as the subsequent initial value problem:

$$ \begin{cases} {}_0^c D_t^\sigma \mathrm{N}(t) + \phi_* \mathrm{N} = \Pi_N, \\ \mathrm{N}(0) = \mathrm{N}_0. \end{cases} \tag{26} $$

When we apply the Laplace transform on both sides, we get

$$ \mathscr{L}\left[\mathrm{N}(t) + \phi_* \mathrm{N}\right] = \mathscr{L}\left[\Pi_N\right]. \tag{27} $$

We get

$$ \mathrm{N}(s) = \frac{s^{-1}(\Pi_N + s^\sigma \mathrm{N}_0)}{s^\sigma + \phi}. \tag{28} $$

From inverse Laplace transform, we get

$$ \begin{aligned} \mathrm{N}(t) &= \Pi_N t^\sigma \mathrm{E}_{\sigma,\sigma+1}(-\phi t^\sigma) + \mathrm{N}_0 \mathrm{E}_{\sigma,\sigma+1}(-\phi t^\sigma) \\ &\leq \frac{\Pi_N}{\phi}\left[\phi t^\sigma \mathrm{E}_{\sigma,\sigma+1}(-\phi t^\sigma)\right] + \mathrm{E}_{\sigma,\sigma+1}(-\phi t^\sigma) \\ &\leq \frac{\Pi_N}{\phi}\frac{1}{\Gamma(1)} \leq \frac{\Pi_N}{\phi}, \end{aligned} \tag{29} $$

where $\mathrm{E}_{\sigma,\sigma+1}$ represents Mittag-Leffler function.

Because the entire population is bounded, the sub-populations are as well, completing the proof. □

Qualitative analysis

Equilibrium points and reproductive number

Lemma 5.1 The equilibrium point of (12) is the solution to the

$$ \begin{aligned} \Pi_N + \upsilon \mathrm{M}_\delta - \alpha \mathrm{F}_N \mathrm{A}_\beta - \phi_1 \mathrm{F}_N &= 0, \\ \alpha \mathrm{F}_N \mathrm{A}_\beta - \beta_1 \mathrm{I}_N \mathrm{M}_\delta - (\gamma + \phi_2)\mathrm{I}_N &= 0, \\ \gamma \mathrm{I}_N - \beta_2 \mathrm{A}_\beta \mathrm{M}_\delta - (d_\beta + \kappa)\mathrm{A}_\beta &= 0, \\ \kappa \mathrm{A}_\beta - \beta_3 \mathrm{T}_\mu \mathrm{M}_\delta - (d_\mu + \rho)\mathrm{T}_\mu &= 0, \\ (\beta_1 \mathrm{I}_N + \beta_2 \mathrm{A}_\beta + \beta_3 \mathrm{T}_\mu)\mathrm{M}_\delta - \phi_3 \mathrm{M}_\delta &= 0. \end{aligned} \tag{30} $$

If every eigenvalue (ϖ_i) of the Jacobian matrix evaluated at the equilibrium point satisfies

$$ |\arg(\varpi_i)| > \frac{\sigma\pi}{2}, $$

then the equilibrium point is locally asymptotically stable.
According to the Lemma 5.1, Eq. (12)'s disease-free equilibrium point is

$$ P^0 = \{\mathrm{F}_N^0,\ \mathrm{I}_N^0,\ \mathrm{A}_\beta^0,\ \mathrm{T}_\mu^0,\ \mathrm{M}_\delta^0\} = \left\{\frac{\Pi_N}{\phi_1}, 0, 0, 0, 0\right\}. \tag{31} $$

Next, the next-generation matrix approach[48,49] is used to calculate the basic reproduction number $(\mathscr{R}_0)$ of Eq. (12). The number of secondary instances of the primary cases that occur during the infectious period as a result of the infection type is known as the basic reproduction number. For this purpose, consider the system

$$ \begin{aligned} {}_0^c D_t^\sigma \mathrm{I}_N(t) &= \alpha \mathrm{F}_N \mathrm{A}_\beta - \beta_1 \mathrm{I}_N \mathrm{M}_\delta - (\gamma + \phi_2)\mathrm{I}_N, \\ {}_0^c D_t^\sigma \mathrm{A}_\beta(t) &= \gamma \mathrm{I}_N - \beta_2 \mathrm{A}_\beta \mathrm{M}_\delta - (d_\beta + \kappa)\mathrm{A}_\beta, \\ {}_0^c D_t^\sigma \mathrm{T}_\mu(t) &= \kappa \mathrm{A}_\beta - \beta_3 \mathrm{T}_\mu \mathrm{M}_\delta - (d_\mu + \rho)\mathrm{T}_\mu. \end{aligned} \tag{32} $$

The associated transition matrix (V) and incidence matrix (F) for the system (12), at P^0, are obtained as follows, respectively:

$$ \mathrm{F} = \begin{pmatrix} 0 & \frac{\alpha \Pi_N}{\phi_1} & 0 \\ 0 & 0 & 0 \\ 0 & 0 & 0 \end{pmatrix}, \quad \mathrm{V} = \begin{pmatrix} \gamma + \phi_2 & 0 & 0 \\ -\gamma & d_\beta + \kappa & 0 \\ 0 & -\kappa & d_\mu + \rho \end{pmatrix}. \tag{33} $$

Then, from spectral radius of FV^{-1}, we have the reproductive number $(\mathscr{R}_0)$ as:

$$\mathscr{R}_0 = \frac{\alpha\gamma\Pi_N}{(\gamma+\phi_2)(d_\beta+\kappa)}. \tag{34}$$

One important epidemiological statistic that is connected to cognitive capacities and the likelihood of incident Alzheimer's disease is the fundamental reproduction number $\mathscr{R}_0$. The risk of incident Alzheimer's disease will be higher if $\mathscr{R}_0 > 1$ and lower if $\mathscr{R}_0 < 1$. In terms of biology, the term "reproductive number $(\mathscr{R}_)$" in Alzheimer's refers to the transmission of misfolded proteins and illness from neuron to neuron or from region to region rather than from person to person. The average number of new neurons or brain regions infected by a pathogenic protein, like tau, that originate from a single infected neuron or region during its infectious phase is indicated here by $\mathscr{R}_0$. When the $\mathscr{R}_0 > 1$, it means that the pathology is gradually expanding and advancing the disease. On the other hand, $\mathscr{R}_0 < 1$ indicates that the pathology is contained and cannot spread further, which could lead to a very sluggish or non-progressive disease state.

Equation (12)'s endemic equilibrium point is $P^* = \{\mathrm{F}_N^*,\ \mathrm{I}_N^*,\ \mathrm{A}_\beta^*,\ \mathrm{T}_\mu^*,\ \mathrm{M}_\delta^*\}$, where

$$\begin{aligned}
\mathrm{F}_N^* &= \frac{\Pi_N + \upsilon \mathrm{M}_\delta^*}{\alpha \mathrm{A}_\beta^* + \phi_1}, \qquad \mathrm{I}_N^* = \frac{\alpha \mathrm{F}_N^* \mathrm{A}_\beta^*}{\beta_1 \mathrm{M}_\delta^* + \gamma + \phi_2},\\
\mathrm{A}_\beta^* &= \frac{\gamma \mathrm{I}_N^*}{\beta_2 \mathrm{M}_\delta^* + d_\beta + \kappa}, \qquad \mathrm{T}_\mu^* = \frac{\kappa \mathrm{A}_\beta^*}{\beta_3 \mathrm{M}_\delta^* + d_\mu + \rho},\\
\mathrm{M}_\delta^* &= \max\left\{ \frac{\alpha \mathrm{F}_N^* \mathrm{A}_\beta^* - (\gamma+\phi_2)\mathrm{I}_N^*}{\beta_1 \mathrm{I}_N^*},\ \frac{\gamma \mathrm{I}_N^* - (d_\beta+\kappa)\mathrm{A}_\beta^*}{\beta_2 \mathrm{A}_\beta^*},\ \frac{\kappa \mathrm{A}_\beta - (d_\mu+\rho)\mathrm{T}_\mu^*}{\beta_3 \mathrm{T}_\mu^*} \right\}.
\end{aligned} \tag{35}$$

P^* exists when $\mathscr{R}_0 > 1$.

Sensitivity of $\mathscr{R}_0$'s parameters

The sensitivity analysis of the $\mathscr{R}_0$ to the parameters in Eq. (38) is presented in this subsection. This analysis's goal is to quantify the factors that most affect $\mathscr{R}_0$. We use normalized sensitivity index[50] and the following formula can be used to get the index of each parameter involved in $\mathscr{R}_0$:

$$\Im_z^{\mathscr{R}_0} = \frac{\partial \mathscr{R}_0}{\partial z}\frac{z}{\mathscr{R}_0}, \tag{36}$$

where $\Im_z^{\mathscr{R}_0}$ is the normalized sensitivity index formula in which z represents the parameter to be analyzed. Table 2 displays the findings of the sensitivity index calculation on the model parameters.

A positive sensitivity index means that higher parameter values result in higher basic reproduction numbers, whereas negative sensitivity means that higher parameter values result in lower basic reproduction numbers. As an illustration, if the sensitivity index is $\Im_\alpha^{\mathscr{R}_0} = 1$, then raising the α value by 10% will raise $\mathscr{R}_0$ by 10%, and if $\Im_{\phi_2}^{\mathscr{R}_0} = -0.5277$, then raising the ϕ_2 value by 10% will reduce $\mathscr{R}_0$ by 5.277%. They thereby help to lower the basic reproduction number, which in turn helps to lower the disease's prevalence. Figure 2 shows a bar graph of these results. Additionally, the sensitivity plots in Fig. 3(a) - 3(g) show how different model parameters affect the $\mathscr{R}_0$.

Ulam-hyres stability

This section goes into the Ulam-Hyers stability of nonlinear fractional-order systems utilizing fractional methods, a concept that dates back to the twentieth century and originated with Ulam and Hyers' work between 1940 and 1941. In numerical analysis and optimization, Ulam-Hyers stability is essential because it yields near-precise results rather than perfect ones. Ulam-Hyers-Rassias has made a substantial contribution to this issue. Simulations that show how small variances in solutions disappear over time can be used to numerically verify Ulam-Hyers stability. This entails proving convergence, comparing perturbed solutions to accurate ones, and offering information about the mathematical model's adaptability and reliability. It ensures that slight variations in initial conditions or external factors do not produce unanticipated results, with the system's response proportionate to the scale of the perturbation. Because of the intrinsic complexity of nonlinear fractional-order models, analytical solutions are frequently unattainable, necessitating reliance on numerical techniques and approximate analytical methods. Proving UH stability for fractional models uses fixed-point theorems within appropriate function spaces, simplifying the approach and eliminating the necessity for Lyapunov analysis. Furthermore, proving Ulam-Hyers stability validates the use of numerical methods by assuring that calculated

Parameter	Sensitivity index	Parameter	Sensitivity index
α	1.0000	Π_N	1.0000
γ	0.4722	ϕ_2	− 0.5277
d_β	− 0.9999	κ	− 0.0026

Table 2. Parameters sensitivity index results.

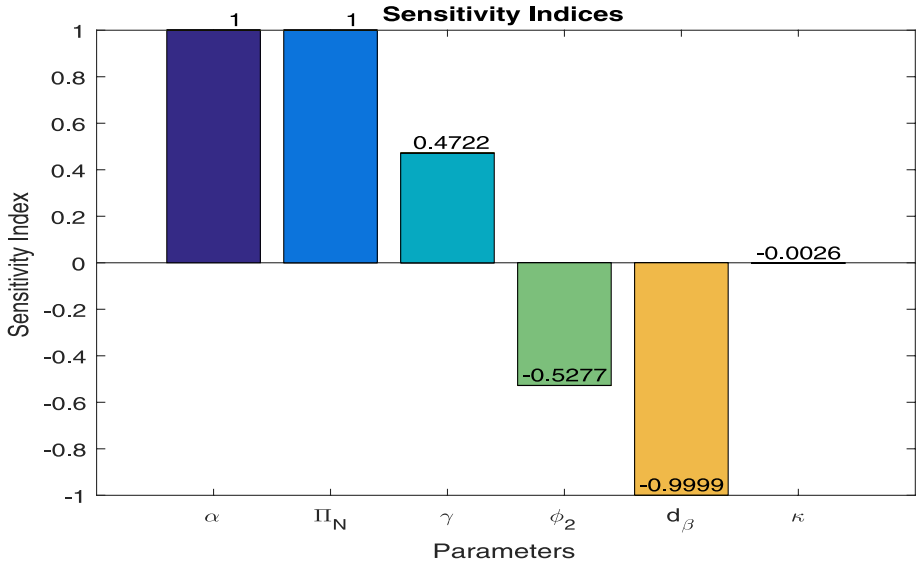

Fig. 2. Sensitivity indices of the $\mathscr{R}_0$'s parameters.

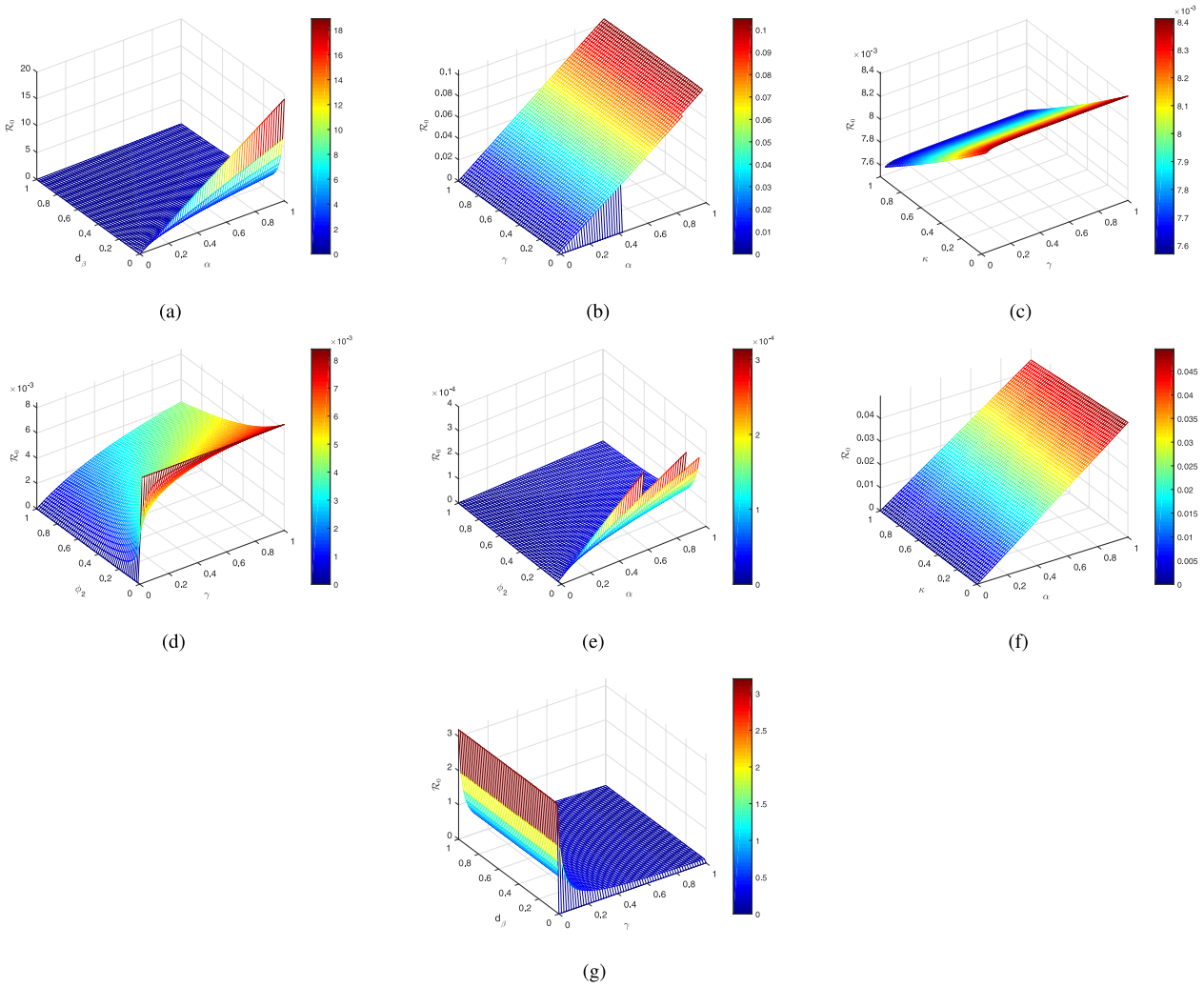

Fig. 3. Variations in $\mathscr{R}_0$ via different parameters.

numerical solutions are consistently close to the genuine but unknown precise solutions of the models, protecting against mathematically nonsensical findings.

Lemma 6.1 The solution of the problem

$$\begin{cases} {}^{c}_{0}D^{\sigma}_{t}Q(t) = \varpi(t, Q(t)) + m(t), \\ Q(0) = Q_0, \end{cases} \tag{37}$$

satisfies the following:

$$\left| Q(t) - Q_0 - \frac{1}{\Gamma(\sigma)} \int_0^t \varpi(\varsigma, Q(\varsigma))(t-\varsigma)d\varsigma \right| \leq \frac{\Im^{\sigma}}{\Gamma(\sigma+1)}\eta = \varphi\eta. \tag{38}$$

Definition 6.1 The system (12) is Ulam-Hyers-Rassias stable for $\eta(t) \in \mathrm{L}^1([0,\mathrm{T}],\mathbb{R})$ and a real valued continuous function $z(t)$ on $[0,\infty)$, provided that

- $\exists$ a real value $\delta_\sigma > 0$, and
- for each of the solutions $(\mathrm{F}_N, \mathrm{I}_N, \mathrm{A}_\beta, \mathrm{T}_\mu, \mathrm{M}_\delta) \in \mathrm{L}^1([0,\mathrm{T}],\mathbb{R})$ of the following inequality

$$\left|{}^{c}_{0}D^{\sigma}_{t}Q(t) - z(t, Q(t))\right| \leq \eta(t), \tag{39}$$

there is a solution $(\bar{\mathrm{F}_N}, \bar{\mathrm{I}_N}, \bar{\mathrm{A}_\beta}, \bar{\mathrm{T}_\mu}, \bar{\mathrm{M}_\delta}) \in \mathrm{L}^1([0,\mathrm{T}],\mathbb{R})$ of (12) satisfying

$$|Q(t) - \bar{Q}(t)| \leq \delta_\sigma \eta(t). \tag{40}$$

Theorem 6.1 The system (12) is Ulam-Hyers-Rassias stable for $\mathrm{L}^1([0,\mathrm{T}],\mathbb{R})$ if

$$QM^{\sigma} < 1. \tag{41}$$

Proof For $\varpi > 0$,

$$\int_0^t (t-\varsigma)\eta(\varsigma)d\varsigma \leq \varpi\eta(t), \qquad \forall t \in [0,\mathrm{T}]. \tag{42}$$

According to Definition 6.1, η is a non-decreasing function of t. It has been demonstrated that the function φ is continuous and that the solutions' positivity satisfies the Lipschitz conditions. Therefore, we have

$$\bar{Q}(t) = Q_0 + \frac{1}{\Gamma(\sigma)} \int_0^t (t-\varsigma)^{\sigma-1} \|z(\varsigma, \bar{Q}(\varsigma))\| d\varsigma. \tag{43}$$

Integrating gives us

$$\left|Q(t) - Q_0 - \frac{1}{\Gamma(\sigma)} \int_0^t (t-\varsigma)^{\sigma-1} z(\varsigma, Q(\varsigma))d\varsigma\right| \leq \frac{1}{\Gamma(\sigma)} \int_0^t (t-\varsigma)^{\sigma-1}\eta(\varsigma)d\varsigma \leq \frac{\varpi M^{\sigma}}{\Gamma(\sigma+1)}\eta(t). \tag{44}$$

Also, we get

$$\begin{aligned} \left|Q(t) - \bar{Q}(t)\right| &\leq \Big|Q(t) - Q_0 - \Big\{\frac{1}{\Gamma(\sigma)} \int_0^t (t-\varsigma)^{\sigma-1} z(\varsigma, \bar{Q}(\varsigma))d\varsigma \\ &\quad + \frac{1}{\Gamma(\sigma)} \int_0^t (t-\varsigma)^{\sigma-1} z(\varsigma, Q(\varsigma))d\varsigma - \frac{1}{\Gamma(\sigma)} \int_0^t (t-\varsigma)^{\sigma-1} z(\varsigma, Q(\varsigma))d\varsigma\Big\}\Big| \\ &\leq \left|Q(t) - Q_0 - \frac{1}{\Gamma(\sigma)} \int_0^t (t-\varsigma)^{\sigma-1} z(\varsigma, Q(\varsigma))d\varsigma\right| \\ &\quad + \frac{1}{\Gamma(\sigma)} \int_0^t (t-\varsigma)^{\sigma-1} \Big|z(\varsigma, Q(\varsigma)) - z(\varsigma, \bar{Q}(\varsigma))\Big| d\varsigma \\ &\leq \frac{\varpi M^{\sigma}\eta(t)}{\Gamma(\sigma+1)} + \frac{\Psi_z M^{\sigma}}{\Gamma(\sigma+1)} \int_0^t (t-\varsigma)^{\sigma-1} \big|Q(\varsigma) - \bar{Q}(\varsigma)\big| d\varsigma \\ &\leq \frac{\varpi M^{\sigma}\eta(t)\mathrm{E}_\sigma(\Psi_z M^{\sigma})}{\Gamma(\sigma+1)}. \end{aligned} \tag{45}$$

Let $\frac{\varpi M^{\sigma}\mathrm{E}_\sigma(\Psi_{\varphi_i} M^{\sigma})}{\Gamma(\sigma+1)} = \delta_\sigma$, then

$$|Q(t) - \bar{Q}(t)| \leq \delta_\sigma \eta(t). \tag{46}$$

□

Chaos control

Adaptive techniques can be used to regulate the chaos in the fractional order system (12) when uncertainties and disturbances are taken into account. The objective is to appropriately build controllers to stabilize chaos around fixed points in the system's trajectories. We use a linear feedback regulate method to stabilize the regulated design of the proposed system (12) based on its equilibrium points.

Theorem 7.1 Under the following control law, the fractional-order chaotic system is stabilized.

$$\begin{aligned}
&{}_0^cD_t^\sigma \mathrm{F}_N(t) = \Pi_N + \upsilon \mathrm{M}_\delta - \alpha \mathrm{F}_N \mathrm{A}_\beta - \phi_1 \mathrm{F}_N - \psi_1(\mathrm{F}_N - \mathrm{F}_N^\star),\\
&{}_0^cD_t^\sigma \mathrm{I}_N(t) = \alpha \mathrm{F}_N \mathrm{A}_\beta - \beta_1 \mathrm{I}_N \mathrm{M}_\delta - (\gamma + \phi_2)\mathrm{I}_N - \psi_2(\mathrm{I}_N - \mathrm{I}_N^\star),\\
&{}_0^cD_t^\sigma \mathrm{A}_\beta(t) = \gamma \mathrm{I}_N - \beta_2 \mathrm{A}_\beta \mathrm{M}_\delta - (d_\beta + \kappa)\mathrm{A}_\beta - \psi_3(\mathrm{A}_\beta - \mathrm{A}_\beta^\star),\\
&{}_0^cD_t^\sigma \mathrm{T}_\mu(t) = \kappa \mathrm{A}_\beta - \beta_3 \mathrm{T}_\mu \mathrm{M}_\delta - (d_\mu + \rho)\mathrm{T}_\mu - \psi_4(\mathrm{T}_\mu - \mathrm{T}_\mu^\star),\\
&{}_0^cD_t^\sigma \mathrm{M}_\delta(t) = (\beta_1 \mathrm{I}_N + \beta_2 \mathrm{A}_\beta + \beta_3 \mathrm{T}_\mu)\mathrm{M}_\delta - \phi_3 \mathrm{M}_\delta - \psi_5(\mathrm{M}_\delta - \mathrm{M}_\delta^\star).
\end{aligned} \tag{47}$$

where $\{\}^\star$ depicts the system (6)'s equilibrium point and control parameters are: $\psi_1; \psi_2; \psi_3; \psi_4, \psi_5$.

Proof The Jacobian matrix at equilibrium point is given as follows:

$$J(P^\star) = \begin{bmatrix}
-\phi_1 - \psi_1 & 0 & -\alpha\frac{\Pi_N}{\phi_1} & \rho & 0\\
0 & -\gamma - \phi_2 - \psi_2 & \alpha\frac{\Pi_N}{\phi_1} & 0 & 0\\
0 & \gamma & -d_\beta - \kappa - \psi_3 & 0 & 0\\
0 & 0 & \kappa & -d_\mu - \rho - \psi_4 & 0\\
0 & 0 & 0 & 0 & -\phi_3 - \psi_5
\end{bmatrix}. \tag{48}$$

The characteristic equation can be expressed as follows:

$$f(\xi) = \begin{vmatrix}
\xi + \phi_1 + \psi_1 & 0 & \alpha\frac{\Pi_N}{\phi_1} & -\rho & 0\\
0 & \xi + \gamma + \phi_2 + \psi_2 & -\alpha\frac{\Pi_N}{\phi_1} & 0 & 0\\
0 & -\gamma & \xi + d_\beta + \kappa + \psi_3 & 0 & 0\\
0 & 0 & -\kappa & \xi + d_\mu + \rho + \psi_4 & 0\\
0 & 0 & 0 & 0 & \xi + \phi_3 + \psi_5
\end{vmatrix} = 0. \tag{49}$$

Letting $\psi_1 = 1$, $\psi_2 = 2$, $\psi_3 = 3$, $\psi_4 = 4$, and $\psi_5 = 5$ gives us

$$\xi_1 = \phi_1 - 1, \qquad \xi_2 = -\gamma - \phi_2 - 2, \qquad \xi_3 = -d_\beta - \kappa - 3, \tag{50}$$

$$\xi_4 = -d_\mu - \rho - 4, \qquad \xi_5 = -\phi_3 - 5. \tag{51}$$

We can easily verify that

$$|\arg \xi_i| = \pi > \frac{\sigma\pi}{2} \quad \text{and} \quad |\xi_i| < \left[2cos\left(\frac{|\arg \xi_i| - \pi}{2 - \sigma}\right)\right]^\sigma, \qquad 0 < \sigma < 1. \tag{52}$$

We can observe that all of the eigenvalues are negative, as shown below, using the parameter values from Table 1, which provides the asymptotic stability for the equilibrium point.

$$\xi_1 = -1.08, \quad \xi_2 = -2.00036, \quad \xi_3 = -12.535, \quad \xi_4 = -4.302, \quad \xi_5 = -5.015. \tag{53}$$

□

Numerical scheme

According to recent research, power-law processes can be simulated using the Caputo derivative. Given the dynamics seen in fractional calculus, we employed the temporal derivative in conjunction with the Caputo derivative to incorporate power law effects into our model. The problem is then discretized using a numerical approach[51,52] based on Newton polynomial interpolation. We can generalize the system (12) in abstract form:

$$\begin{cases}
{}_0^cD_t^\sigma Q(t) = \lambda(t, Q(t)), & \sigma \in (0, 1], \quad t \in [0, \mathrm{T}],\\
Q(0) = Q_0,
\end{cases} \tag{54}$$

Then we have

$$Q(\mathrm{t}_{\zeta+1}) = Q_0 + \frac{1}{\Gamma(\sigma)} \sum_{j=2}^{\zeta} \int_{t_j}^{\mathrm{t}_{j+1}} \lambda(\mathrm{t}_{\zeta+1} - \varsigma)^{\sigma-1} d\varsigma. \tag{55}$$

Approximating $\lambda(t, \Delta(t))$ using the Newton polynomial as

$$\begin{aligned} \mathrm{P}_l(\phi) \simeq\ & \lambda(t_{j-2}, Q^{j-2}) \\ & + \frac{1}{Qt} \left[\lambda(t_{j-1}, Q^{j-1}) - \lambda(t_{j-2}, Q^{j-2})\right] \times (\phi - t_{j-2}) \\ & + \frac{1}{2Qt^2} \left[\lambda(t_j, Q^j) - 2\lambda(t_{j-1}, Q^{j-1}) + \lambda(t_{j-2}, Q^{j-2})\right] \times (\phi - t_{j-2})(\phi - t_{j-1}). \end{aligned} \tag{56}$$

After some computations, we get

$$\begin{aligned} Q(\mathrm{t}_{\zeta+1}) = Q_0 & + \frac{(\Delta t)^\sigma}{\Gamma(\sigma+1)} \sum_{j=2}^{\zeta} \lambda(\mathrm{t}_{j-2}, Q^{j-2}) \times \left((\zeta - j + 1)^\sigma - (\zeta - j)^\sigma\right) \\ & + \frac{(\Delta t)^\sigma}{\Gamma(\sigma+2)} \sum_{j=2}^{\zeta} \left\{\lambda(\mathrm{t}_{j-1}, Q^{j-1}) - \lambda(\mathrm{t}_{j-2}, Q^{j-2})\right\} \times \begin{pmatrix} (\zeta - j + 1)^\sigma (\zeta - j + 3 + 2\sigma) \\ -(\zeta - j)^\sigma (\zeta - j + 3(1+\sigma)) \end{pmatrix} \\ & + \frac{\sigma(\Delta t)^\sigma}{2\Gamma(\sigma+3)} \sum_{j=2}^{\zeta} \left\{\lambda(\mathrm{t}_j, Q^j) - 2\lambda(\mathrm{t}_{j-1}, Q^{j-1}) + \lambda(\mathrm{t}_{j-2}, Q^{j-2})\right\} \\ & \times \begin{pmatrix} (\zeta - j + 1)^\sigma \{2(\zeta - j)^2 + (3\sigma + 10)(\zeta - j) + (2\sigma + 9)\sigma + 12\} \\ -(\zeta - l)^\sigma \{2(\zeta - j)^2 + (5\sigma + 10)(\zeta - j) + 6(\sigma^2 + 3\sigma + 2)\}. \end{pmatrix} \end{aligned} \tag{57}$$

The proposed scheme's algorithm is illustrated in Fig. 4.

Simulations discussion

This section investigates the temporal dynamics of our fractional-order model, revealing a variety of shifting patterns in different compartments and providing numerical evidence to support our findings. Using the Newton polynomial method described in the previous section, we mathematically examine the effects of fractional order changes on the density of functioning neurons, infected neurons, amyloid-beta, tau protein and microglia. The values of the parameters are taken from Table 1. We used MATLAB programming to run these simulations. The analysis shows consistent behavior patterns and a substantial correlation between the dynamics of the fractional-order and integer-order models. The inquiry centers on various fractional order cases, all of which are available through the figures. Numerical results are derived for various ways of assessing the feasibility and accuracy of the proposed model, as shown in Figures 6-19, which support theoretical observations. Details of each sub-figure are also explained below for better representation and understanding of the behavior of the model.

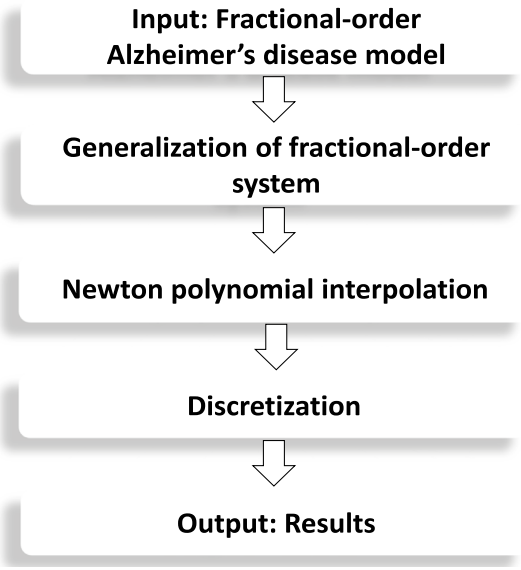

Fig. 4. Numerical scheme's algorithm.

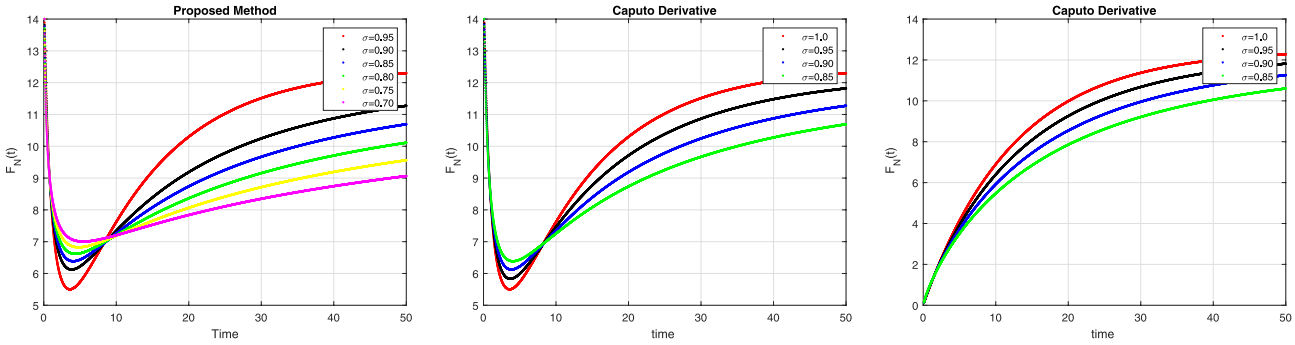

(a) (b) (c)

Fig. 5. Comparison results of $\mathrm{F}_N(t)$ using integer-order, fractional-order and different population.

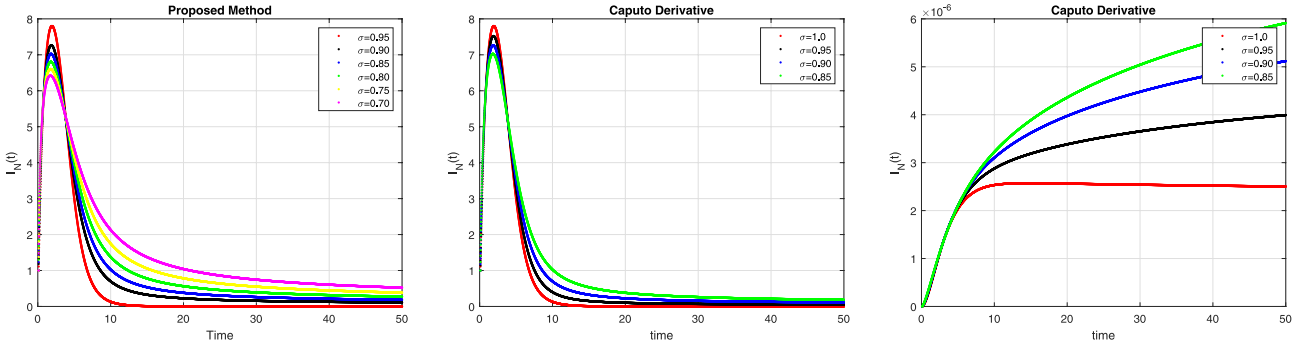

(a) (b) (c)

Fig. 6. Comparison results of $\mathrm{I}_N(t)$ using integer-order, fractional-order and different population.

- Fig. 5a shows the analysis of functioning neurons at various σ levels. We see that functional neurons first decline in the presence of harmful proteins and then resume normal functioning once microglia are activated. The comparison study of integer-order and fractional-order model is displayed in Fig. 5b. At larger fractional orders, we observe an increase in functioning neurons. Using actual data from the literature, Fig. 5c illustrates the dynamics of $\mathrm{F}_N(t)$ at different σ levels. At increasing σ values, we observe an increase in functioning neurons.
- The study of infected neurons at different σ levels is shown in Fig. 6a. Infected neurons accumulate as a result of the infection, and as they recover, they start to deteriorate and stabilize. Figure 6b shows the comparison study of the integer-order and fractional-order models. The density of tau and amyloid-beta proteins, as well as infected neurons, noticeably decreases at increasing fractional orders. Figure 6c shows the dynamics of $\mathrm{I}_N(t)$ at various σ values using real data from the literature. The dynamics of infected neurons decrease more quickly at large σ values than at high fractional orders.
- Figure 7a displays the amyloid-beta analysis at different σ values. Amyloid-beta protein levels gradually decline as a result of microglia activation. The comparative study between the fractional-order and integer-order models is shown in Fig. 7b. The density of amyloid-beta decreases noticeably with higher fractional orders. The dynamics of $\mathrm{A}_\beta(t)$ at various σ values are depicted in Fig. 7c using real data from the literature. Compared to high fractional orders, the dynamics of A_β decrease more quickly for large σ values.
- The simulation of tau protein at different σ levels is shown in Fig. 8a. High σ values cause the tau protein's dynamics to drop more quickly than high fractional orders. Figure 8b shows the comparison study of the integer-order and fractional-order models. The tau protein density noticeably decreases with higher fractional orders. Figure 8c shows the dynamics of $\mathrm{T}_\mu(t)$ at various σ values using real data from the literature. The dynamics of T_μ decrease more quickly at large σ values than they do at high fractional orders.
- In Fig. 9a, microglia are analyzed at different σ levels. Microglia first become more functional at high fractional orders, but thereafter their functionality declines at high fractional orders. In Fig. 9b, the comparison study of integer-order and fractional-order models is shown. Microglia proliferate more rapidly at low fractional orders than at higher fractional orders and integer-order order. The dynamics of $\mathrm{M}_\delta(t)$ at various σ values are depicted in Fig. 9c using real data from the literature. Microglia's performance decreases at large fractional orders in contrast to smaller σ values.
- When it comes to representing memory and hereditary characteristics in biological systems, a Caputo fractional model performs better than conventional integer-order models. These effects are crucial for examining

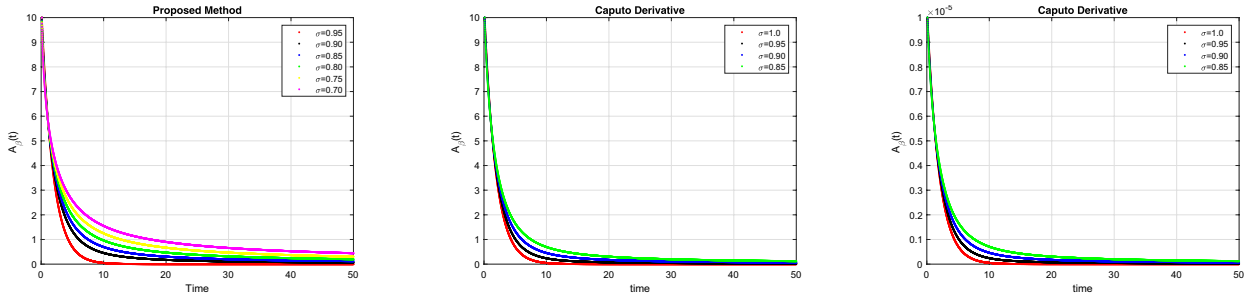

(a) Different fractional-orders (b) Comparison with integer-order (c) Different population

Fig. 7. Comparison results of $\mathrm{A}_{\beta}(t)$ using integer-order, fractional-order and different population.

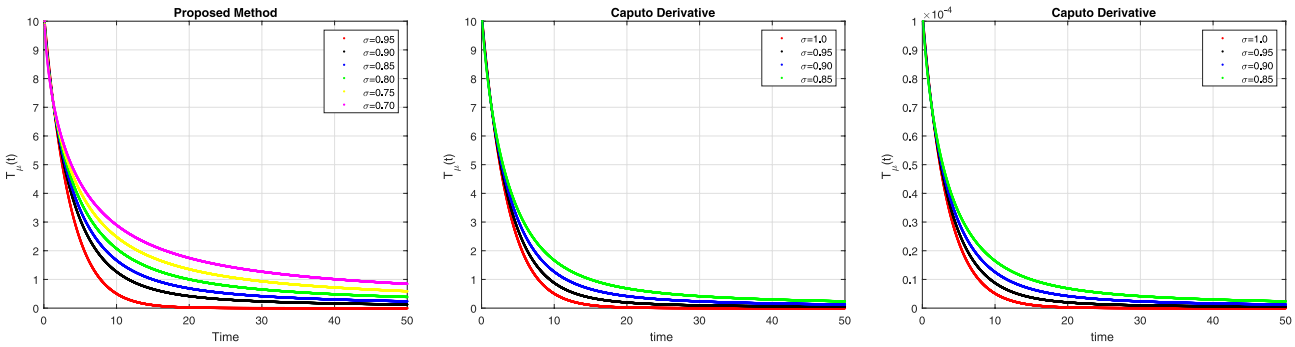

(a) (b) (c)

Fig. 8. Comparison results of $\mathrm{T}_{\mu}(t)$ using integer-order, fractional-order and different population.

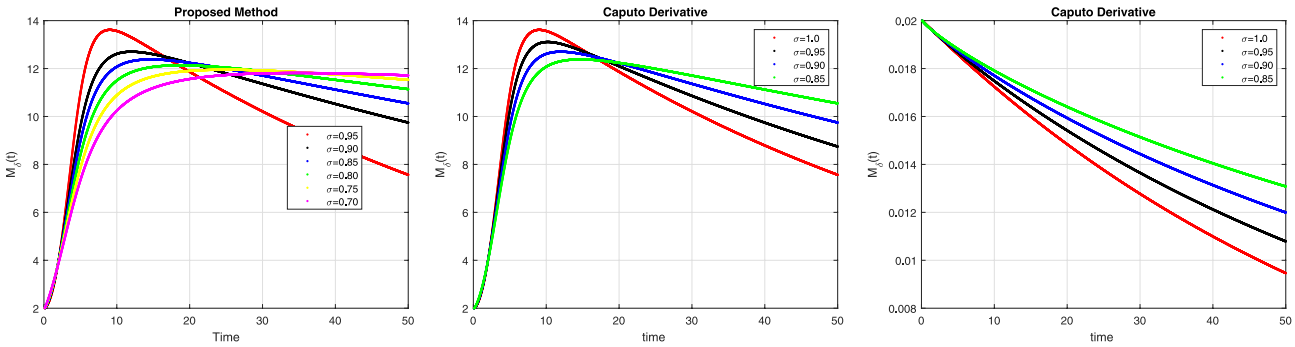

(a) (b) (c)

Fig. 9. Comparison results of $\mathrm{M}_{\delta}(t)$ using integer-order, fractional-order and different population.

the course of Alzheimer's disease. The Caputo derivative is preferred among fractional approaches because it can include integer-order initial conditions. It is especially useful for expressing phenomena with nonlocal features because of this capability. The non-locality of the Caputo fractional operator illustrates the role of memory in the dynamics of Alzheimer's disease. Its spectrum of low to high prevalence is analyzed to determine its efficacy. The fractional order σ in the fractional model of Alzheimer's disease characterizes memory or time-delay effects, illustrating how past states affect disease dynamics. A smaller σ indicates a stronger memory effect, which is dependent on the disease's complete history, whereas values near 1 indicate lesser memory and behavior, similar to standard integer-order differential equations. This technique helps describe the complicated, non-local temporal dynamics of Alzheimer's disease, such as amyloid-β build-up and Microglia activation. The conventional integer order model solution at $\sigma = 1$ is used in the study to compare integer-order results with numerical simulation results. Over longer time periods, curves with $\sigma = 0.95, 0.90, 0.85$ exhibit a slower increase or decrease. A fair ratio can be employed to lessen the conse-

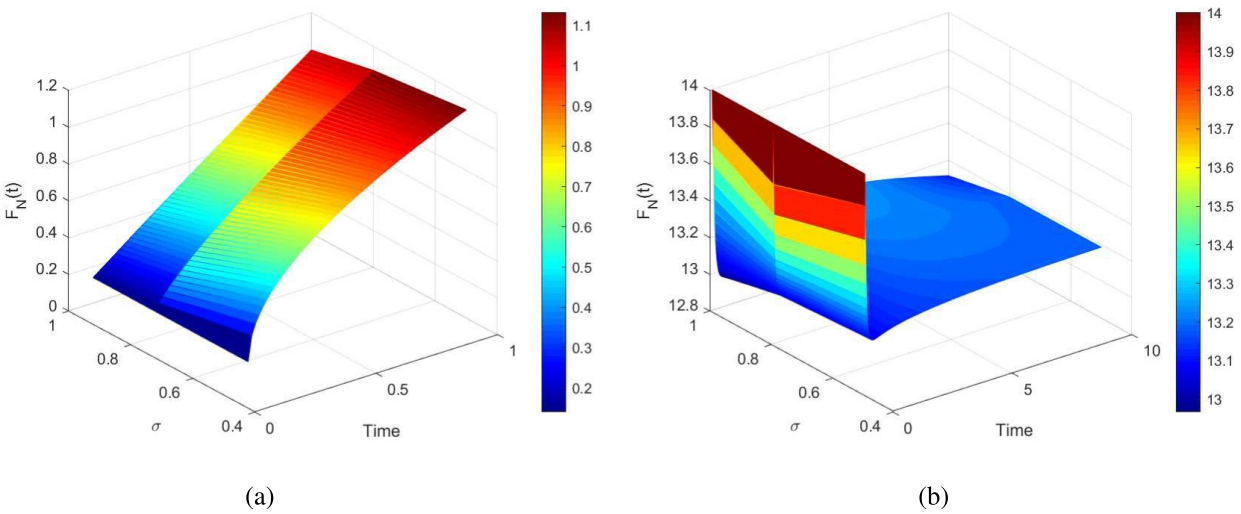

Fig. 10. Response surface plot of $\mathrm{F}_N(t)$.

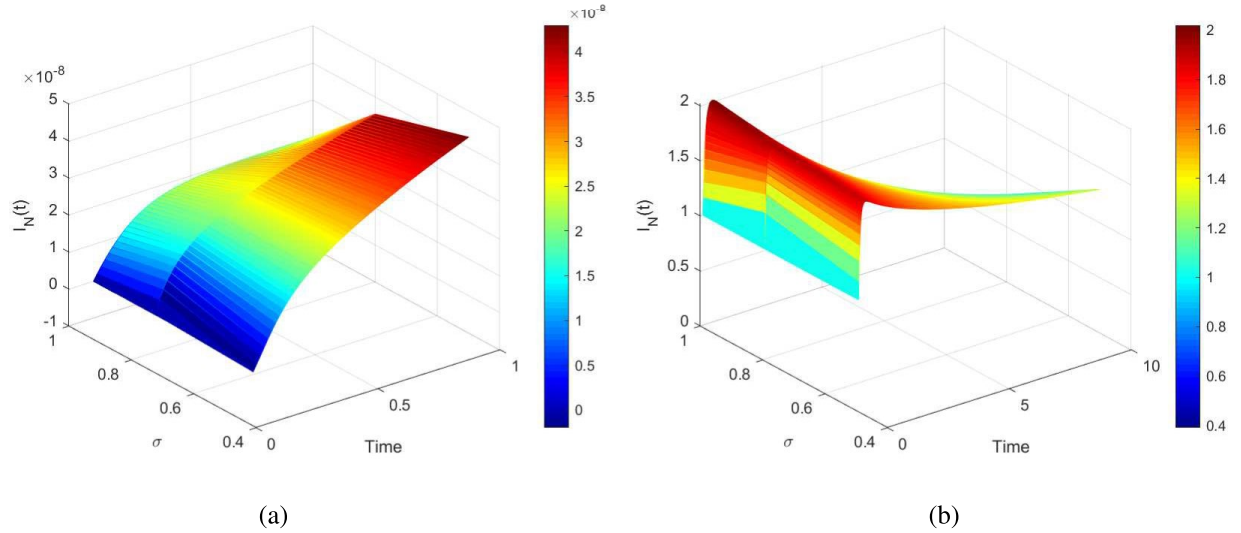

Fig. 11. Response surface plot of $\mathrm{I}_N(t)$.

quences of amyloid beta and tau protein. With the system's memory effect and derivative order decreasing from 1, the concentration of tau and amyloid-beta proteins rises, suggesting that fractional-order dynamics with memory effects are more robust. For long-range interactions between neurons, amyloid-beta, tau protein, infected neurons, and microglia, the model provides more accurate predictions. Effective therapy of Alzheimer's disease requires an understanding of its historical dynamics.

- A surface plot shows a three-dimensional relationship in two dimensions with variables on the two axes and a smooth surface. Figure 10a and b show 3D surface graphs for functional neurons with suggested parameter values and different population, respectively. Figure 11a and b show 3D surface graphs for infected neurons with suggested parameter values and different population, respectively. Figure 12a and b show 3D surface graphs for amyloid-beta concentration with suggested parameter values and different population, respectively. Figure 13a and b show 3D surface graphs for tau protein concentration with suggested parameter values and different population, respectively. Figure 14a and b show 3D surface graphs for microglia density with suggested parameter values and different population, respectively. Surface plots of the feasible zone's stable relation and the chaos region for various compartments in the phase trajectory are displayed. These response surface plots show the main effects and interaction effects of independent variables. The idea that fractional derivatives influence neuron concentration is supported by variations in outlines. Compartment densities are shown by surface peaks.

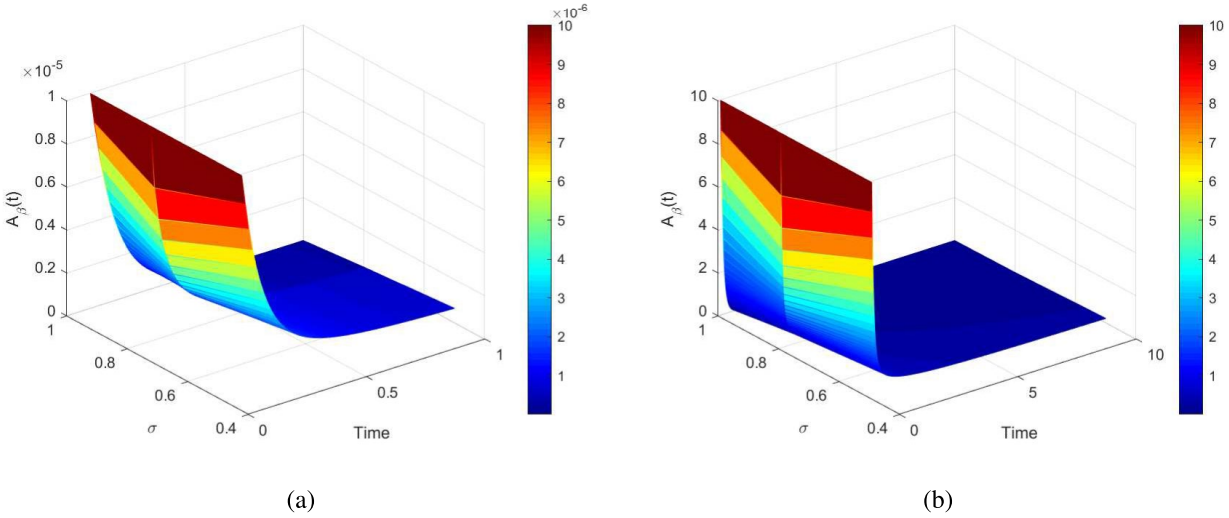

Fig. 12. Response surface plot of $\mathrm{A}_{\beta}(t)$.

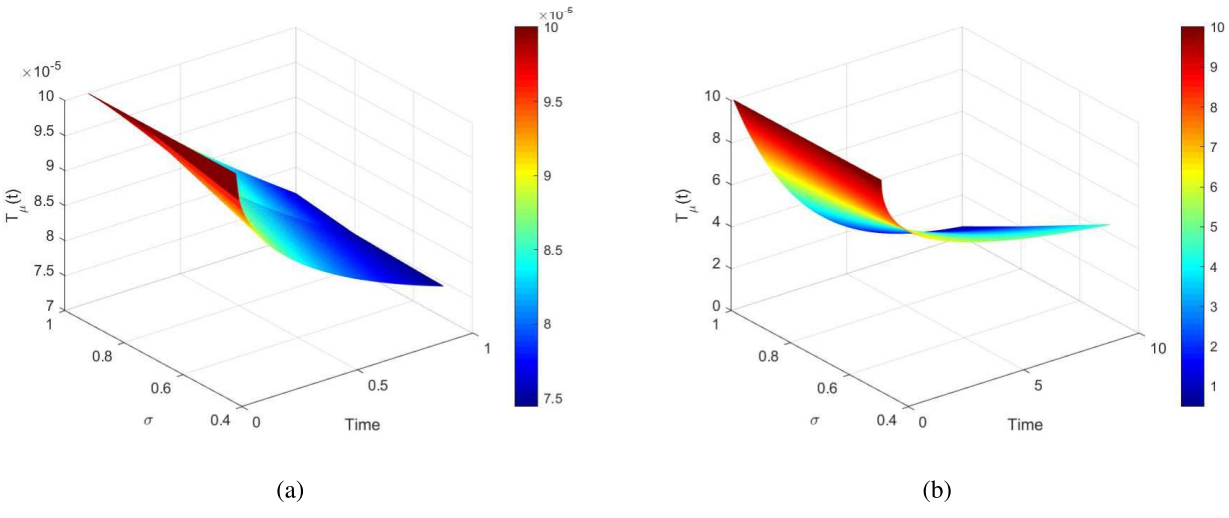

Fig. 13. Response surface plot of $\mathrm{T}_{\tau}(t)$.

- Two-dimensional contour plots give visual representations of response values. A contour plot joins points with the same response value to show a two-dimensional representation of a response variable. Contour plots for functioning neurons with recommended parameter values and distinct populations are displayed in Fig. 15a and b, respectively. Contour plots for infected neurons with varied populations and recommended parameter values are displayed in Fig. 16a and b. Contour plots for amyloid-beta concentration with recommended parameter values and distinct populations are displayed in Fig. 17a and b, respectively. Contour plots for tau protein concentration with recommended parameter values and distinct populations are displayed in Fig. 18a and b, respectively. Contour plots for microglia density with recommended parameter values and distinct populations are displayed in Fig. 19a and b, respectively. These contour plots show stepwise behavior and reveal fractional order σ for each compartment. For compartment densities as shown by contour plots, darker areas imply slower progression and lighter patches indicate higher densities.

The comparative numerical outcomes for all biological compartments associated with Alzheimer's disease (AD) under integer-order conditions are presented in Tables 3, 4, 5, 6 and 7. Table 3 illustrates the temporal evolution of the F_N compartment, representing the population of normal neurons. The results indicate that neuronal activity initially increases but gradually declines over time, reflecting the progressive nature of neuronal degradation characteristic of AD. Table 4 presents the results for the I_N compartment, which corresponds to infected or impaired neurons. A noticeable decline is observed for lower fractional values, signifying that diminished memory effects suppress the progression of neuronal impairment. The dynamic response of the A_{β} compartment, shown in Table 5, demonstrates a steady decrease in amyloid-beta concentration over time,

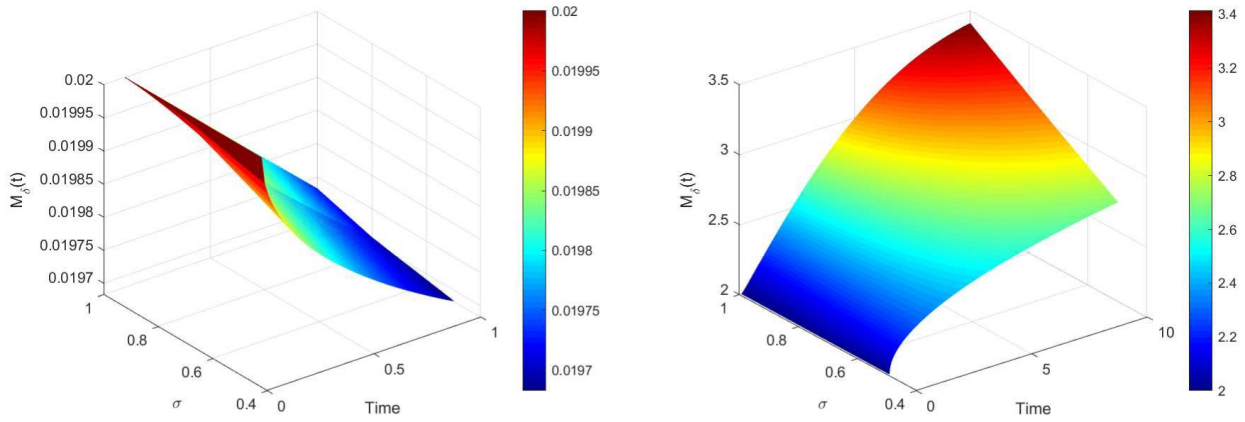

(a) (b)

Fig. 14. Response surface plot of $\mathrm{M}_\delta(t)$.

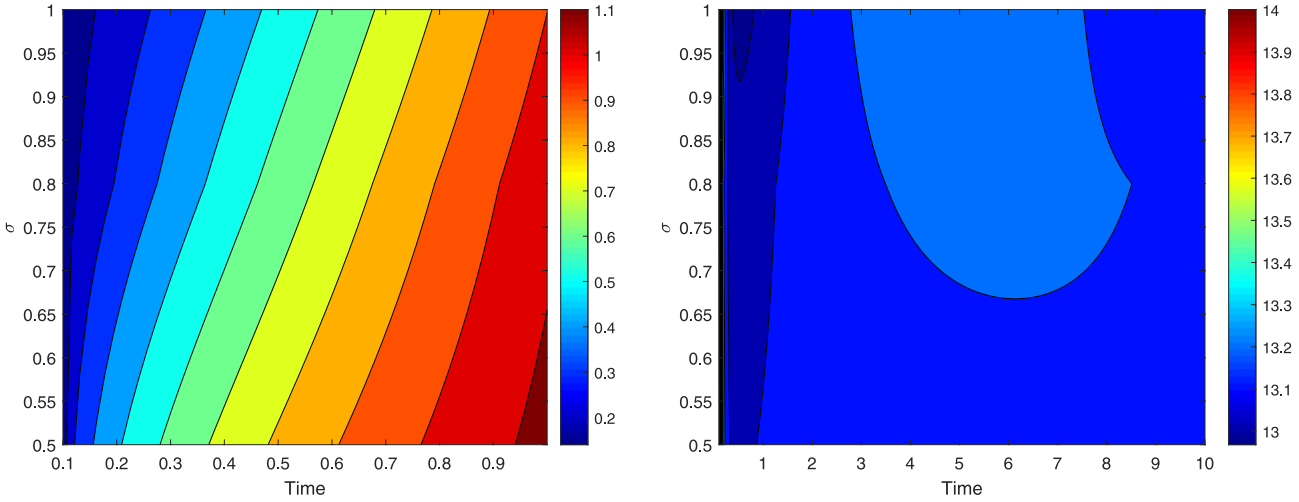

(a) (b)

Fig. 15. Contour plot of $\mathrm{F}_N(t)$ within feasible domain.

implying that the integer-order case promotes a faster clearance mechanism compared to fractional dynamics. Similarly, Table 6 reports the variations in the T_μ compartment, representing activated microglial cells. Here, smaller fractional parameters yield faster decay and lower steady-state values, highlighting the sensitivity of microglial activation to the order of differentiation. Finally, Table 7 summarizes the M_δ compartment results, which describe the density of pro-inflammatory cytokines. The integer-order condition yields the highest magnitude, whereas fractional parameters closer to zero correspond to reduced inflammatory responses.

Conclusion

A novel mathematical model of Alzheimer's disease has been introduced, which includes nonlinear fractional differential equations for tau protein, amyloid-beta, microglia, infected neurons, and functioning neurons. The study analyzed the dynamics of a proposed model for Alzheimer's disease transmission using the next-generation technique. It found two equilibrium points and subjected reproductive number parameters to sensitivity analysis. The study confirmed the Ulam-Hyers-Rassias stability requirements. The model was solved using Newton polynomial interpolation and the discretization of the Caputo fractional-order operator. Simulations were conducted to investigate the global effects of factors on generating circumstances that prevent Alzheimer's disease incidence. Fractional calculus has proven to be a helpful tool for understanding the complex dynamics associated with memory disorders and cognitive deficits in Alzheimer's disease research. Better illness prediction and treatment design are made possible by the analysis, which shows that fractional-order models accurately depict health processes. According to the simulation results, the concentration of tau and amyloid-beta

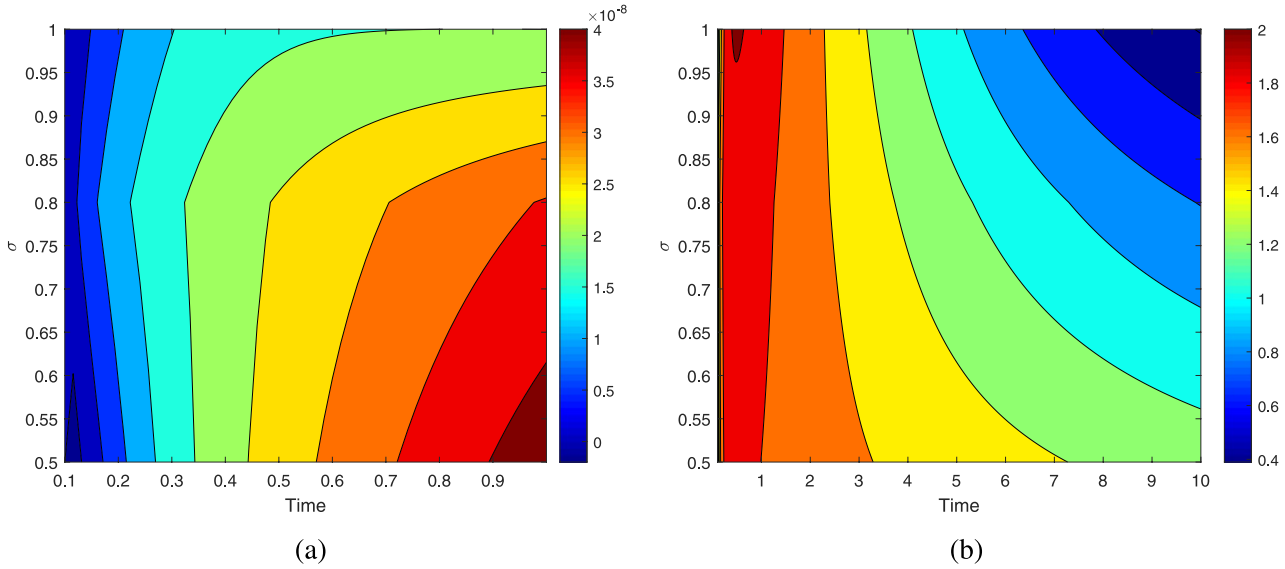

Fig. 16. Contour plot of $\mathrm{I}_N(t)$ within feasible domain.

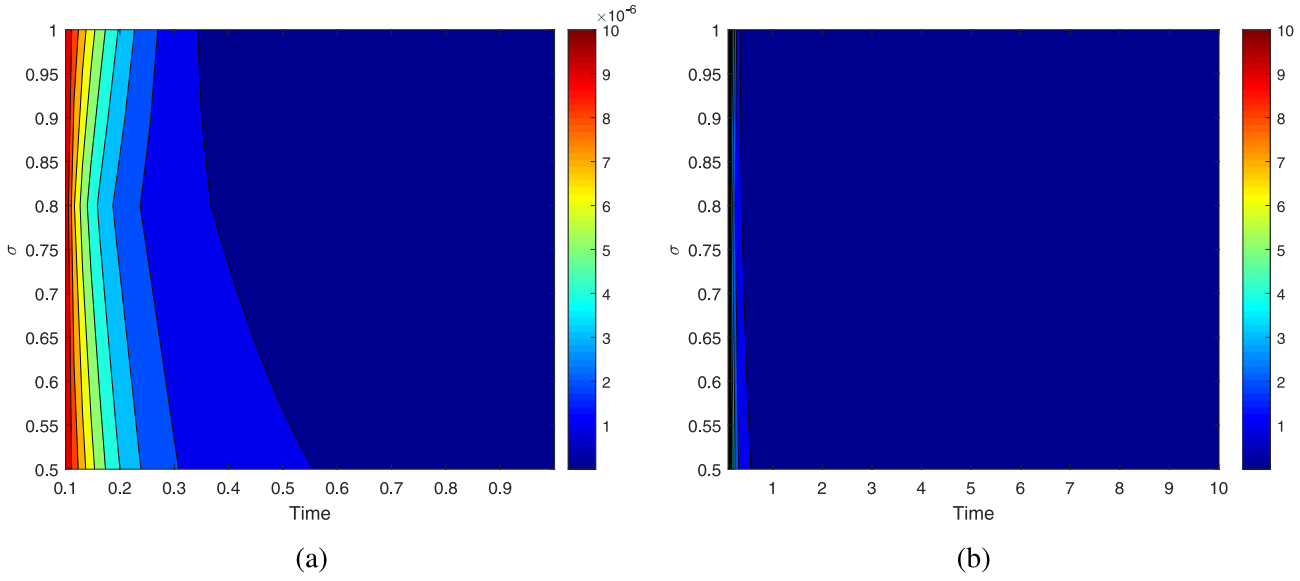

Fig. 17. Contour plot of $\mathrm{A}_\beta(t)$ within feasible domain.

proteins rises with derivative order and memory impact. By tracking changes in treatment controls and illness impacts over time, researchers can improve the design of their models. For increased accuracy, future research recommends including time delay in model dynamics. Validation of real-world data will help improve parameter estimations for useful applications. Collecting statistics on Alzheimer's disease is difficult since patients' cognitive deficits limit communication and self-reporting. The disease's gradual growth makes tracking its development difficult, and variable diagnosis techniques result in untrustworthy data. Ethical concerns about disadvantaged groups provide moral quandaries for researchers, while logistical challenges such as patient accessibility, data sharing issues, and funding limits impede complete data collection. Our model uses arbitrary parameter values identified in the literature, with some values assumed, limiting its applicability to clinical practice. Accurate and interpretable parameters are required for models to provide important insights for early identification and effective treatment. A worldwide data format for normalizing and standardizing measures could greatly improve data integration, making future cohort studies more efficient. This would save researchers a tremendous amount of time. Furthermore, emerging computer modeling methodologies may address present issues in Alzheimer's disease modeling, thereby assisting in the development of medical interventions and procedures. Furthermore, Alzheimer's disease models can be improved by including treatment effects and stochastic disturbances, resulting

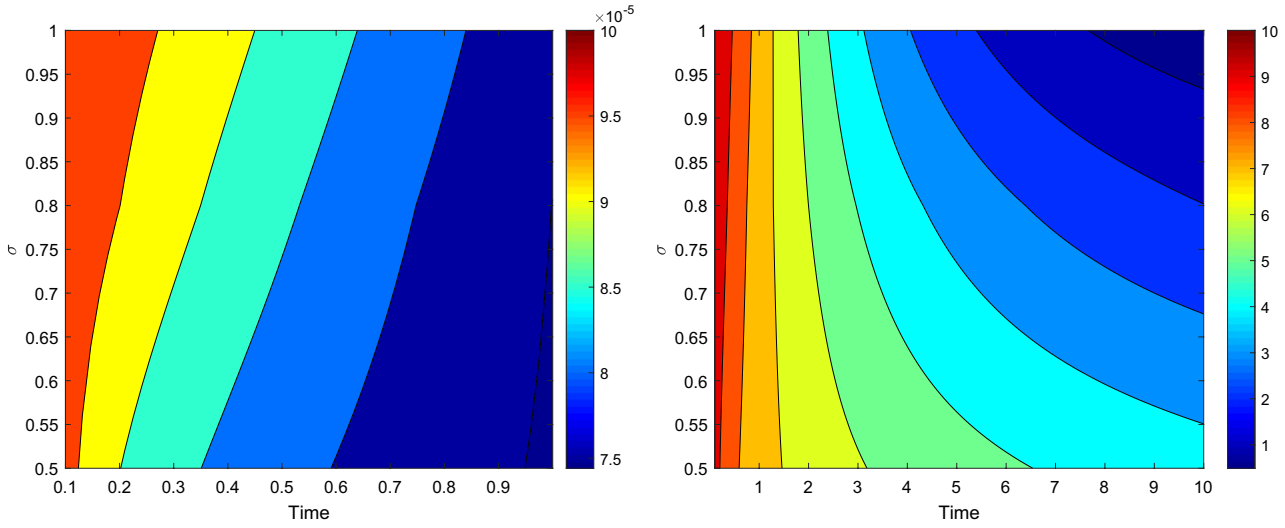

Fig. 18. Contour plot of $\mathrm{T}_{\tau}(t)$ within feasible domain.

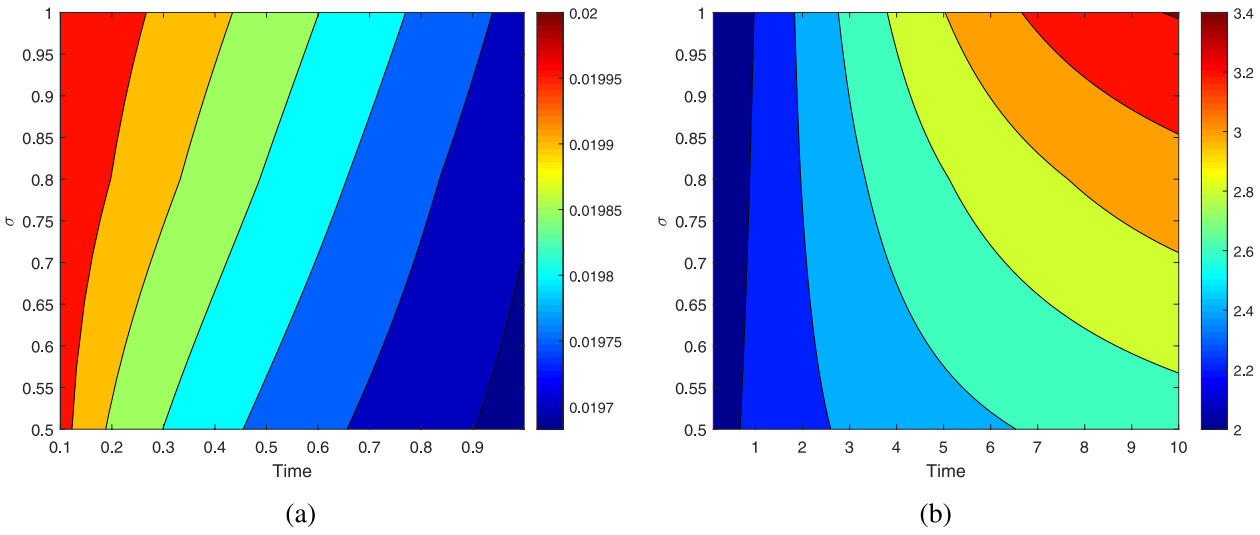

Fig. 19. Contour plot of $\mathrm{M}_{\delta}(t)$ within feasible domain.

t	$\sigma = 1$	$\sigma_1 = 0.95$	$\sigma_2 = 0.90$	$\sigma_3 = 0.85$
10	7.5899	7.4407	7.3228	7.2400
15	9.1911	8.7509	8.3749	8.0667
20	10.2838	9.6972	9.1752	8.7269
25	11.0153	10.3726	9.7778	9.2470
30	11.5050	10.8594	10.2372	9.6615
35	11.8330	11.2144	10.5925	9.9965
40	12.0529	11.4762	10.8712	10.2710
45	12.2003	11.6714	11.0926	10.4985
50	12.2991	11.8187	11.2704	10.6892

Table 3. Comparative analysis of the $F_N(t)$ dynamics obtained under integer-order.

t	$\sigma = 1$	$\sigma_1 = 0.95$	$\sigma_2 = 0.90$	$\sigma_3 = 0.85$
10	0.1394	0.4102	0.7134	1.0441
15	0.0095	0.1527	0.3286	0.5383
20	0.0008	0.1013	0.2268	0.3803
25	0.0001	0.0812	0.1818	0.3057
30	0.0000	0.0701	0.1561	0.2619
35	0.0000	0.0630	0.1393	0.2328
40	0.0000	0.0580	0.1273	0.2119
45	0.0000	0.0543	0.1183	0.1961
50	0.0000	0.0515	0.1114	0.1837

Table 4. Comparative analysis of the $I_N(t)$ dynamics obtained under integer-order.

t	$\sigma = 1$	$\sigma_1 = 0.95$	$\sigma_2 = 0.90$	$\sigma_3 = 0.85$
10	0.0501	0.2408	0.4595	0.7034
15	0.0035	0.1118	0.2523	0.4253
20	0.0002	0.0734	0.1741	0.3056
25	0.0000	0.0554	0.1340	0.2401
30	0.0000	0.0448	0.1095	0.1988
35	0.0000	0.0377	0.0929	0.1702
40	0.0000	0.0326	0.0808	0.1493
45	0.0000	0.0287	0.0716	0.1332
50	0.0000	0.0257	0.0644	0.1204

Table 5. Comparative analysis of the $A_\beta(t)$ dynamics obtained under integer-order.

t	$\sigma = 1$	$\sigma_1 = 0.95$	$\sigma_2 = 0.90$	$\sigma_3 = 0.85$
10	0.5183	0.8949	1.2849	1.6849
15	0.1080	0.3680	0.6689	1.0059
20	0.0225	0.1972	0.4205	0.6910
25	0.0047	0.1296	0.3008	0.5209
30	0.0010	0.0969	0.2340	0.4177
35	0.0002	0.0780	0.1921	0.3493
40	0.0000	0.0657	0.1635	0.3010
45	0.0000	0.0569	0.1427	0.2650
50	0.0000	0.0504	0.1268	0.2371

Table 6. Comparative analysis of the $T_\mu(t)$ dynamics obtained under integer-order.

t	$\sigma = 1$	$\sigma_1 = 0.95$	$\sigma_2 = 0.90$	$\sigma_3 = 0.85$
10	13.5683	13.1011	12.5989	12.0572
15	12.7835	12.7319	12.6005	12.3793
20	11.8758	12.1072	12.2331	12.2416
25	11.0194	11.4754	11.8044	11.9938
30	10.2234	10.8692	11.3693	11.7116
35	9.4847	10.2939	10.9430	11.4188
40	8.7994	9.7501	10.5303	11.1253
45	8.1636	9.2367	10.1332	10.8356
50	7.5737	8.7524	9.7522	10.5518

Table 7. Comparative analysis of the $M_\delta(t)$ dynamics obtained under integer-order.

in more realistic simulations. This method exposes how random variability drives illness progression and how different therapies can alter these dynamics, potentially changing the results reached from the models.

Data availability

The datasets generated during and/or analysed during the current study are available from the corresponding author on reasonable request.

Received: 31 August 2025; Accepted: 22 December 2025
Published online: 07 January 2026

References

1. Uhl, G. R. & Grow, R. W. The burden of complex genetics in brain disorders. *Arch. General Psychiatry* **61**(3), 223–229 (2004).
2. Rockne, R., Alvord, E. C., Rockhill, J. K. & Swanson, K. R. A mathematical model for brain tumor response to radiation therapy. *J. Math. Biol.* **58**, 561–578 (2009).
3. Kostelich, E. J. et al. Accurate state estimation from uncertain data and models: an application of data assimilation to mathematical models of human brain tumors. *Biol. Direct* **6**, 1–20 (2011).
4. Chen, Y., Yin, P., Chen, Q., Zhang, Y., Tang, Y., Jin, W., & Yu, L. (2025). Neurodegenerative diseases and immune system: From pathogenic mechanism to therapy. *Neural Regen. Res.*, 10-4103.
5. Li, Y. et al. Mitochondria-targeting fluorescent sensor with high photostability and permeability for visualizing viscosity in mitochondrial malfunction, inflammation, and AD models. *Anal. Chimica Acta* **1250**, 340967 (2023).
6. Alzheimer's Association. 2015 Alzheimer's disease facts and figures. *Alzheimer's Dementia*, **11**(3), 332-384 (2015). https://doi.org/10.1016/j.jalz.2015.02.003
7. Hampel, H. et al. Biomarkers for Alzheimer's disease: academic, industry and regulatory perspectives. *Nat. Rev. Drug Discov.* **9**(7), 560–574 (2010).
8. Zhang, Y. & Wang, W. Mathematical analysis for stochastic model of Alzheimer's disease. *Commun. Nonlinear Sci. Numeric. Simul.* **89**, 105347 (2020).
9. Puri, I. K. & Li, L. Mathematical modeling for the pathogenesis of Alzheimer's disease. *PloS One* **5**(12), e15176 (2010).
10. Stallard, E. et al. Estimation and validation of a multiattribute model of Alzheimer disease progression. *Med. Decision Making* **30**(6), 625–638 (2010).
11. Britschgi, M. et al. Modeling of pathological traits in Alzheimer's disease based on systemic extracellular signaling proteome. *Mole. Cell. Proteomics* **10**(10), M111-008862 (2011).
12. Han, L. et al. Apelin-13-mediated upregulation of METTL3 ameliorates Alzheimer's disease via inhibiting neuroinflammation through m6A-dependent regulation of lncRNA BDNF-AS. *Biomolecules* **15**(8), 1188 (2025).
13. Anastasio, T. J. Data-driven modeling of Alzheimer disease pathogenesis. *J. Theoretical Biol.* **290**, 60–72 (2011).
14. Helal, M., Hingant, E., Pujo-Menjouet, L. & Webb, G. F. Alzheimer's disease: analysis of a mathematical model incorporating the role of prions. *J. Math. Biol.* **69**(5), 1207–1235 (2014).
15. Bertsch, M., Franchi, B., Marcello, N., Tesi, M. C. & Tosin, A. Alzheimer's disease: a mathematical model for onset and progression. *Math. Med. Biol. J. IMA* **34**(2), 193–214 (2017).
16. Wu, B., Xiao, Q., Zhu, L., Tang, H. & Peng, W. Icariin targets p53 to protect against ceramide-induced neuronal senescence: implication in Alzheimer's disease. *Free Radical Biol. Med.* **224**, 204–219 (2024).
17. Li, S. W., Kuang, Z. D. & Kuang, W. P. Protective effect of gastrodin on dopaminergic neurons by miR-24 targeting of the DJ-1/Nrf2 pathway in Parkinson's disease. *Int. J. Clin. Exp. Med.* **13**(10), 7527–7535 (2020).
18. Petrella, J. R., Hao, W., Rao, A. & Doraiswamy, P. M. Computational causal modeling of the dynamic biomarker cascade in Alzheimer's disease. *Comput. Math. Methods Med.* **2019**(1), 6216530 (2019).
19. Bertsch, M., Franchi, B., Meacci, L., Primicerio, M. & Tesi, M. C. The amyloid cascade hypothesis and Alzheimer's disease: a mathematical model. *Eur. J. Appl. Math.* **32**(5), 749–768 (2021).
20. Hao, W., Lenhart, S. & Petrella, J. R. Optimal anti-amyloid-beta therapy for Alzheimer's disease via a personalized mathematical model. *PLoS Comput. Biol.* **18**(9), e1010481 (2022).
21. Kumari, R., Goel, S., & Das, S. Mathematical modelling of dendritic complexity mechanism in Alzheimer's disease. In *AIP Conference Proceedings* Vol. 2872, No. 1. (AIP Publishing, 2023, September).
22. Rabiei, K., Petrella, J. R., Lenhart, S., Liu, C., Doraiswamy, P. M., & Hao, W. Data-Driven Modeling of Amyloid-beta Targeted Antibodies for Alzheimer's Disease. arXiv preprint. (2025). arXiv:2503.08938.
23. Olayiwola, M. O. & Oluwafemi, E. A. Modeling Tuberculosis Dynamics with Awareness and Vaccination Using Laplace-Adomian and Fractional Calculus. *Iran J. Sci.* (2025). https://doi.org/10.1007/s40995-025-01830-0
24. Olayiwola, M. O., Tijani, K. R., Ogunniran, M. O. et al., Modeling the booster vaccine effect on new COVID-19 variant management employs the Atangana-Baleanu-Caputo fractional derivative operator together with the Laplace-Adomian decomposition method. *Vacunas* **26**(3), 500458 (2025). https://doi.org/10.1016/j.vacun.2025.500458
25. Olayiwola, M. O. & Oluwafemi, E. A. Hereditary and Antimicrobial Factor Shaping Extracellular Bacteria Dynamics in an In-Host Mathematical Model of Tuberculosis for Disease Control. *Tuberculosis* **154**, 102668 (2025).
26. Zarin, R., Humphries, U. W. & Saleewong, T. Advanced mathematical modeling of hepatitis B transmission dynamics with and without diffusion effect using real data from Thailand. *Eur. Phys. J. Plus* **139**(5), 385 (2024).
27. Ivanescu, M., Dumitrache, I., Popescu, N. & Popescu, D. Fractional order model identification of a person with Parkinson's disease for wheelchair control. *Fractal Fract.* **7**(1), 23 (2022).
28. Zarin, R., Guedri, K., Ibrahim, S. M., Alburaikan, A., Khalifa, H. A. E. W., & Nadar, Z. Nonlinear dynamics of measles and HIV co-infection using a reaction-diffusion model and artificial neural networks, *Nonlinear Dyn.* **113**, 26899–26923 (2025).
29. Guedri, K., Zarin, R., Oreijah, M., Alharbi, S. K. & Khalifa, H. A. E. W. Artificial neural network-driven modeling of Ebola transmission dynamics with delays and disability outcomes, *Comput. Biol. Chem.* **115**, 108350 (2025).
30. Zarin, R. Artificial neural network-based approach for simulating influenza dynamics: A nonlinear SVEIR model with spatial diffusion. *Eng. Anal. Boundary Elements* **176**, 106230 (2025).
31. Drapaca, C. S. A mathematical investigation of sex differences in Alzheimer's disease. *Fractal Fract.* **6**(8), 457 (2022).
32. Khan, Z. A., Waqar, M., Chaudhary, N. I., Raja, M. J. A. A., Khan, S., Khan, F. A. & Raja, M. A. Z. Fractional gradient optimized explainable convolutional neural network for Alzheimer's disease diagnosis. *Heliyon* **10**(20), e39037 (2024).
33. Bandyopadhyay, B. & Kamal, S. *Stabilization and Control of Fractional Order Systems: A Sliding Mode Approach*. (Springer, 2014).
34. Raizah, Z. & Zarin, R. Advancing COVID-19 understanding: Simulating omicron variant spread using fractional-order models and haar wavelet collocation. *Mathematics* **11**(8), 1925 (2023).
35. Caputo, M. & Fabrizio, M. A new definition of fractional derivative without singular kernel. *Progress Fract. Differ. Appl.* **1**(2), 73–85 (2015).
36. Haidong, Q., Rahman, M. U. & Arfan, M. Fractional model of smoking with relapse and harmonic mean type incidence rate under Caputo operator. *J. Appl. Math. Comput.* **69**(1), 403–420 (2023).

37. Hardy, J. The relationship between amyloid and tau. *J. Mole. Neurosci.* **20**, 203–206 (2003).
38. Garbuz, D. G., Zatsepina, O. G. & Evgen'ev, M. B. Beta amyloid, tau protein, and neuroinflammation: an attempt to integrate different hypotheses of Alzheimer's disease pathogenesis. *Mole. Biol.* **55**, 670–682 (2021).
39. Valiukas, Z., Tangalakis, K., Apostolopoulos, V., & Feehan, J. Microglial activation states and their implications for Alzheimer's disease. *J. Prev. Alzheimer's Dis.* **12**, 100013 (2025).
40. Subramanian, N., Watson, B., Li, C. Z., Moss, M. & Liu, C. Patterning amyloid-β aggregation under the effect of acetylcholinesterase using a biological nanopore-an in vitro study. *Sens. Act. Rep.* **6**, 100170 (2023).
41. Mehl, L. C., Manjally, A. V., Bouadi, O., Gibson, E. M. & Tay, T. L. Microglia in brain development and regeneration. *Development* **149**(8), dev200425 (2022).
42. Seeman, P. & Seeman, N. Alzheimer's disease: β-amyloid plaque formation in human brain. *Synapse* **65**(12), 1289–1297 (2011).
43. Saido, T. & Leissring, M. A. Proteolytic degradation of amyloid β-protein. *Cold Spring Harbor Perspect.Med.* **2**(6), a006379 (2012).
44. Hao, W. & Friedman, A. Mathematical model on Alzheimer's disease. *BMC Syst. Biol.* **10**, 1–18 (2016).
45. Petrella, J. R., Hao, W., Rao, A. & Doraiswamy, P. M. Computational causal modeling of the dynamic biomarker cascade in Alzheimer's disease. *Comput. Math. Methods Med.* **2019**(1), 6216530 (2019).
46. Dwivedi, A. & Verma, S. Dynamical study of a fear-influenced fractional predator-prey model with disease spread. *Eur. Phys. J. Plus* **140**(4), 306 (2025).
47. Joshi, H. & Yavuz, M. Transition dynamics between a novel coinfection model of fractional-order for COVID-19 and tuberculosis via a treatment mechanism. *Eur. Phys. J. Plus* **138**(5), 468 (2023).
48. Diekmann, O., Heesterbeek, J. A. P. & Roberts, M. G. The construction of next-generation matrices for compartmental epidemic models. *J. Royal Soc. Interface* **7**(47), 873–885 (2010).
49. Ghannam, M. Dynamical transmission of Varicella Virus in Jordan with SVIR Model through analysis and numerical simulations. *J. Math. Model. Fract. Calculus* **1**(2), 72–89 (2025).
50. Chitnis, N., Hyman, J. M. & Cushing, J. M. Determining important parameters in the spread of malaria through the sensitivity analysis of a mathematical model. *Bull. Math. Biol.* **70**, 1272–1296 (2008).
51. Shehzad, A., Jamil, S. & Sarfraz, F. Dynamics of a Food Chain Model Using the Caputo Fractional Derivative. *J. Math. Model. Fracti. Calculus* **2**(1), 39–54 (2025).
52. Atangana, A. Mathematical model of survival of fractional calculus, critics and their impact: How singular is our world?. *Adv. Diff. Equ.* **2021**(1), 403 (2021).

Acknowledgements

The authors extend their appreciation to Prince Sattam bin Abdulaziz University for funding this research work through the project number (PSAU/2025/01/32210).

Author contributions

Conceptualization:KSN, MF; Formal analysis: KSN; Investigation: KSN, MF S; Methodology: MF; Software: KSN, MF; Supervision: KSN; Validation: KSN; Visualization: MF; Writing - original draft: KSN, MF

Funding

None.

Declarations

Competing interests

The authors declare no competing interests.

Additional information

Correspondence and requests for materials should be addressed to K.S.N.